International Collaboration on Advanced Neutron Sources (ICANS XXIV)

Unveiling local magnetic correlations: the development of magnetic pair distribution function at CSNS

Long Yang (杨龙)
Tongji University

About me

- 2011-2015 Fudan University B.S.
- 2015-2016 Columbia University M.S.
- 2017-2021 Columbia University Ph.D.
- 2017-2020 Oak Ridge National Lab Joint Ph.D.
- 2021-2022 UCLA Postdoc
- 2022-Now Tongji University Assistant Professor

Acknowledgements

Simon Billinge
Columbia Univ.

Matthew Tucker
ORNL

Benjamin Frandsen
Brigham Young Univ.

Wen Yin
CSNS

https://yanglonggroup.com

CSNS, Dongguan, China

SNS, ORNL, USA

Collaborators:

- Juping Xu (CSNS)
- Yanzhong Pei (Tongji Univ.)
- He Lin (SSRF)
- Emil Bozin (BNL)
- Yuanpeng Zhang (SNS)
- Matthew Krogstad (ANL)
- …

Structure-Property

Atomic Structure

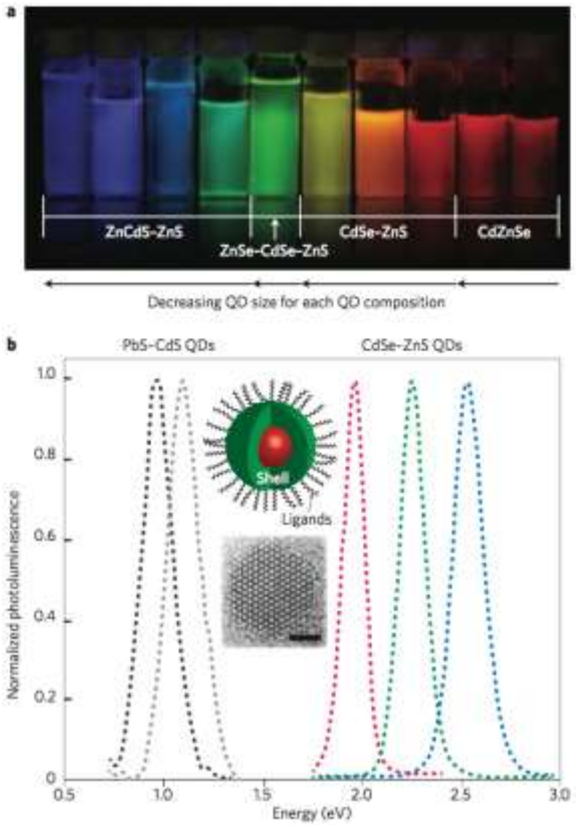

Tunable optical properties in quantum dots

Y. Shirasaki, et al. *Nat. Photonics* 2013, 7, 1.

Magnetic Structure

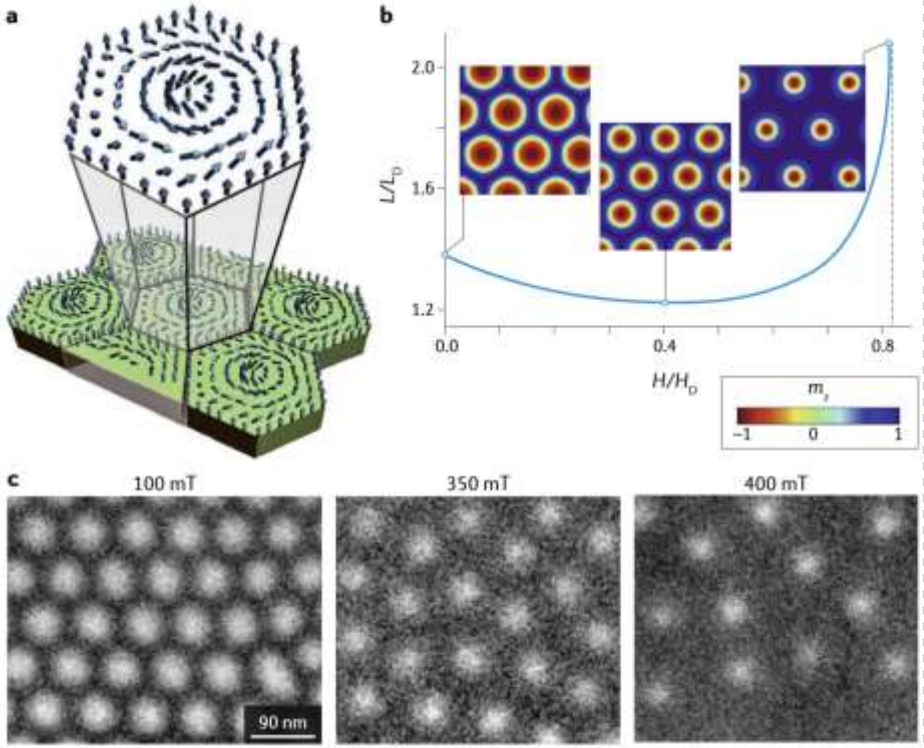

Magnetic skyrmions for spintronic applications

A. Bogdanov and C. Panagopoulos. *Nat. Rev. Phys.* 2020, 2, 9.

Neutron diffraction

Neutrons

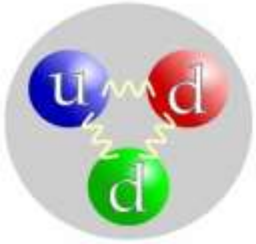

Complementray to x-rays

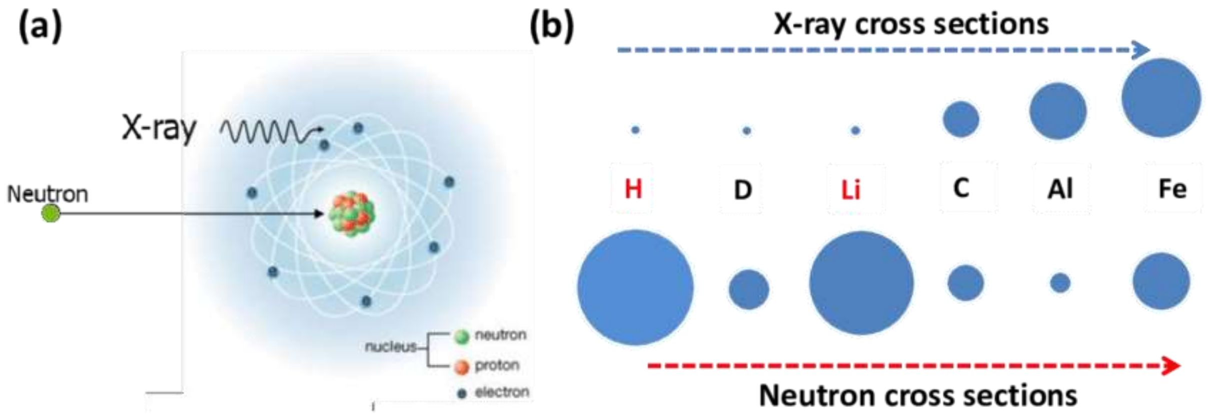

Revealing magnetic structures

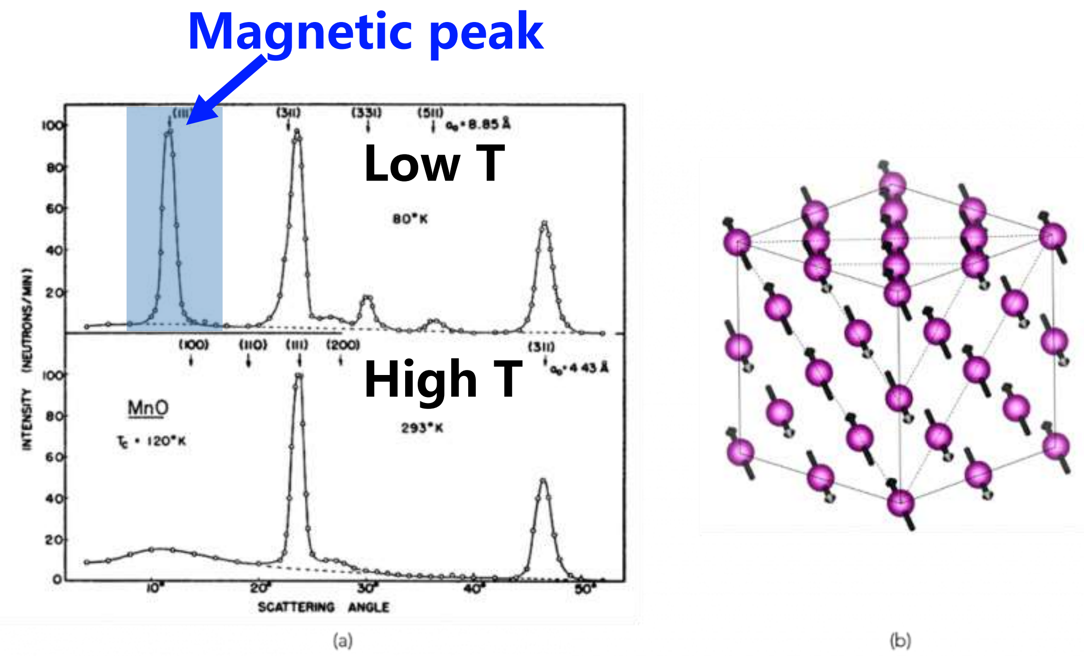

Magnetic structures

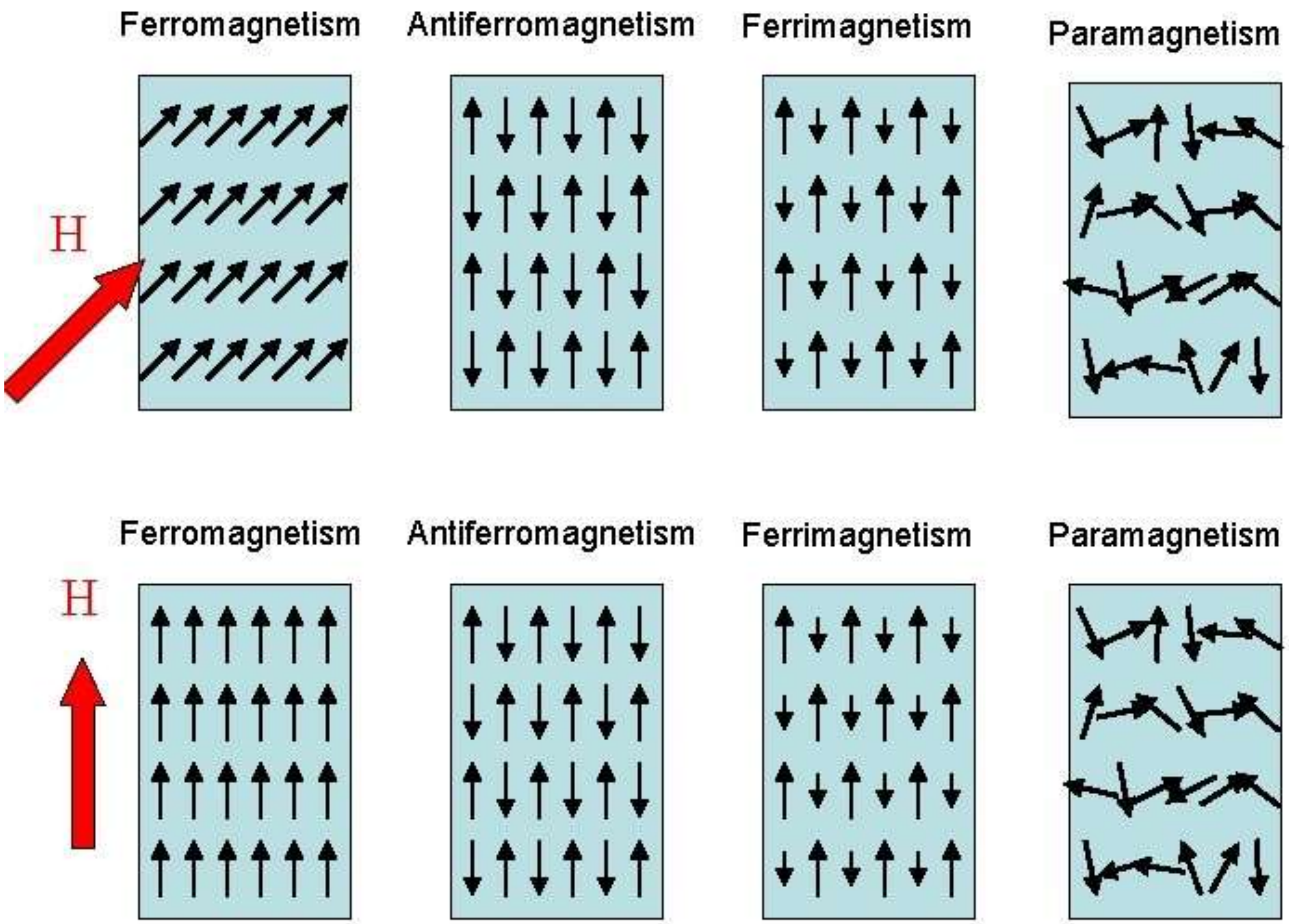

MnO

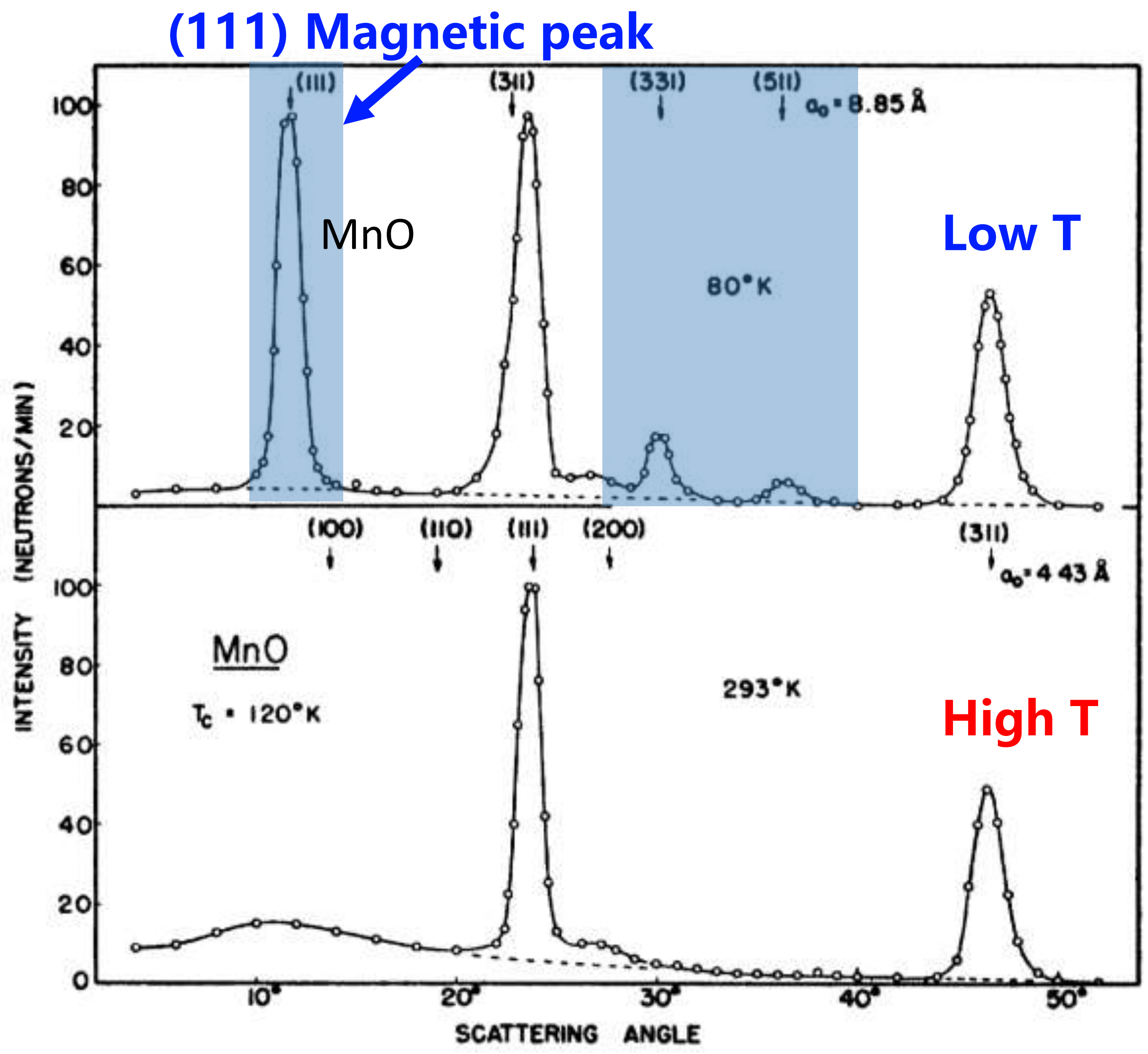

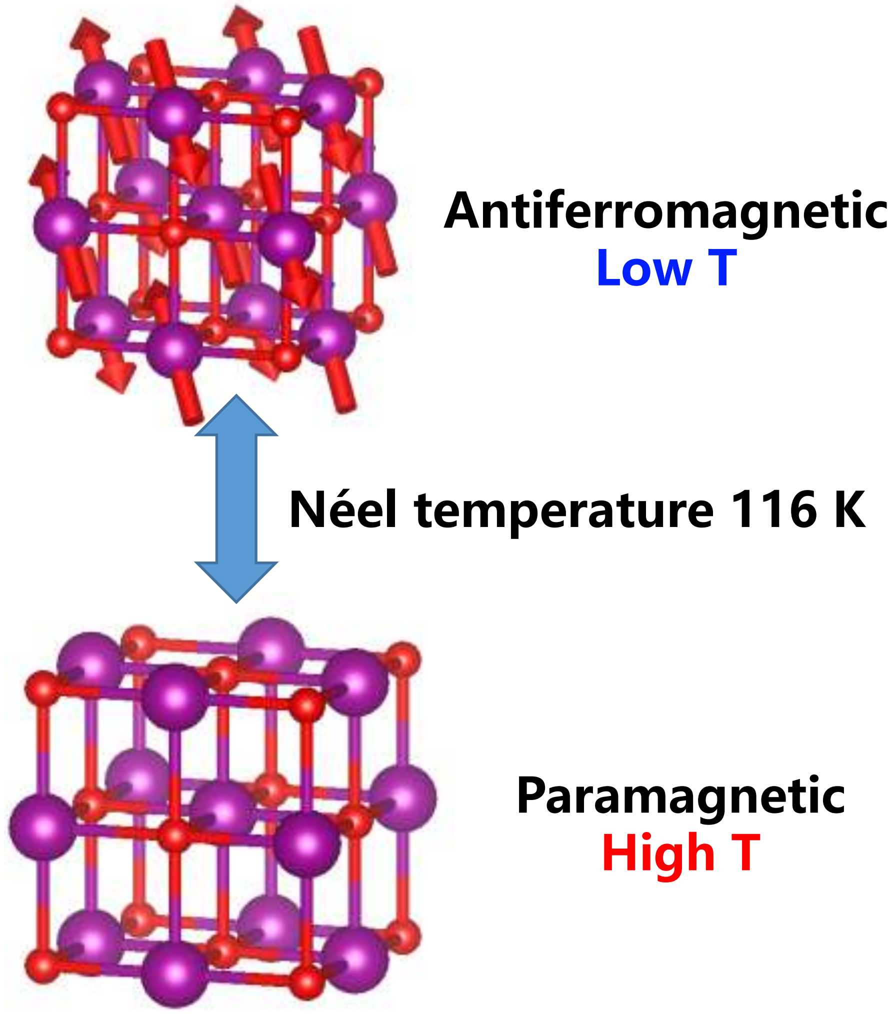

C. G. Shull, W. A. Strauser, and E. O. Wollan. *Phys. Rev.* 1951, 83, 2.

Local magnetic structure

- **The short-range local magnetic correlations are important for understanding exotic properties in advanced condensed matters.**

Spin fluctuations in frustrated magnetism

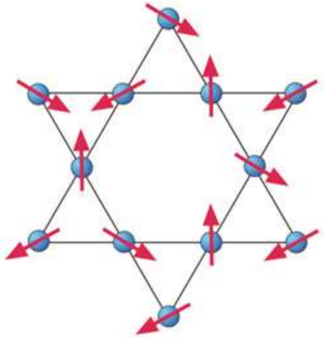

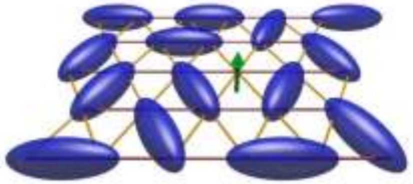

Spinstripe correlations in cuprate superconductors

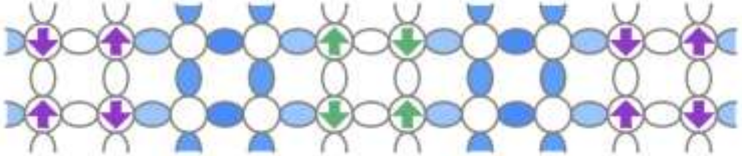

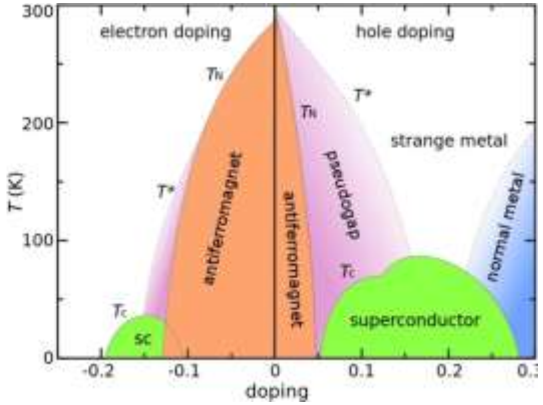

Spin order in diluted magnetic semiconductors

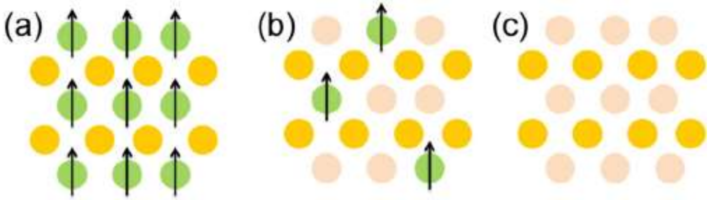

Local structure probe

Conventional diffraction

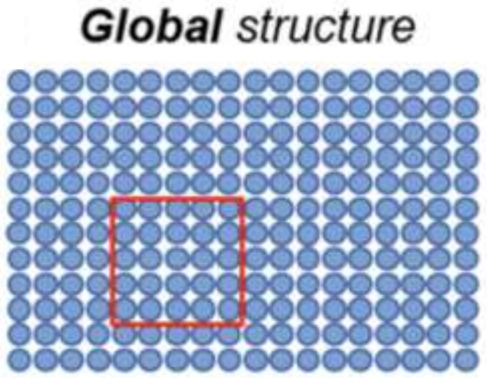

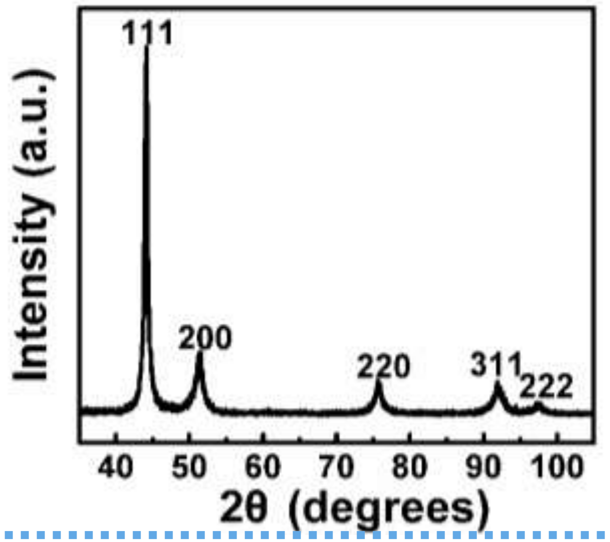

Pair distribution function

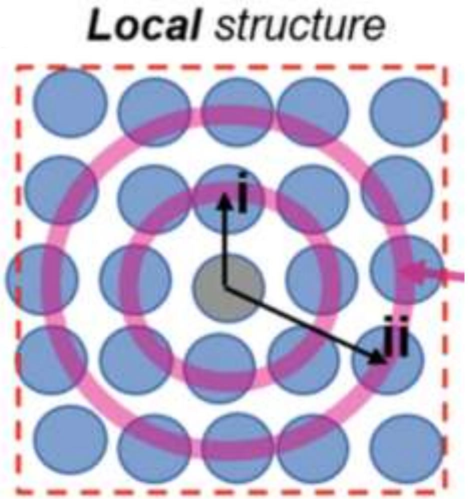

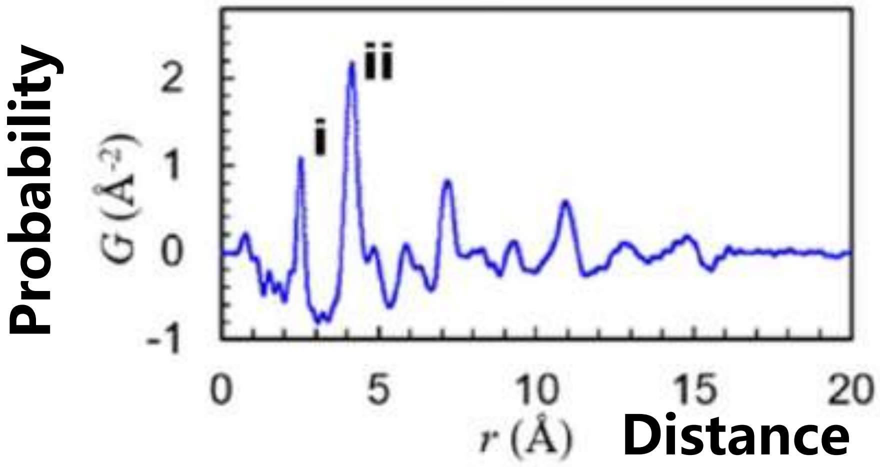

Local structure probe

- **Total scattering technique**

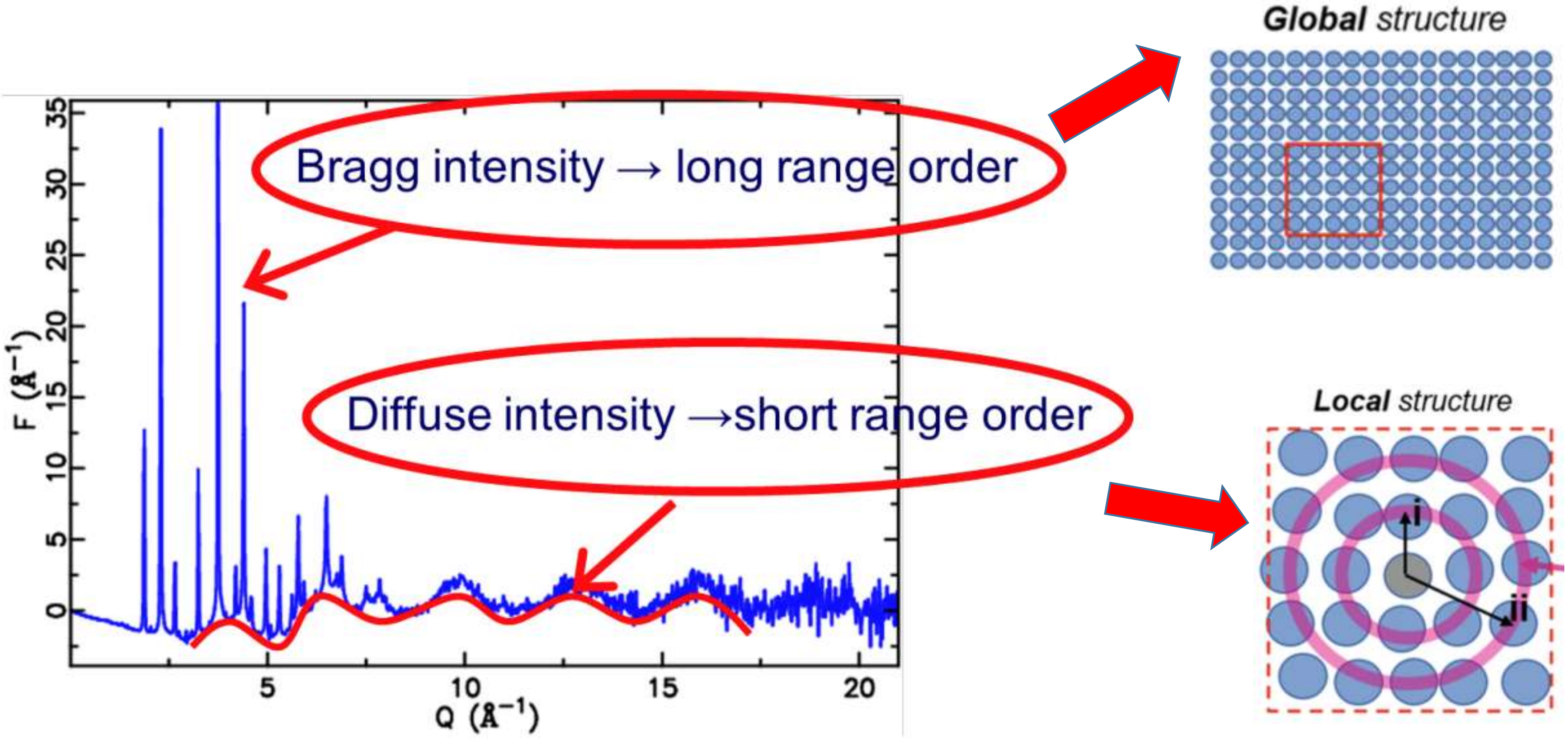

Pair Distribution Function (PDF)

- **Local structure probe.**
- **PDF gives the probability of finding an atom at a distance “r” from a given atom.**
- **Neutron, x-ray, electron.....**

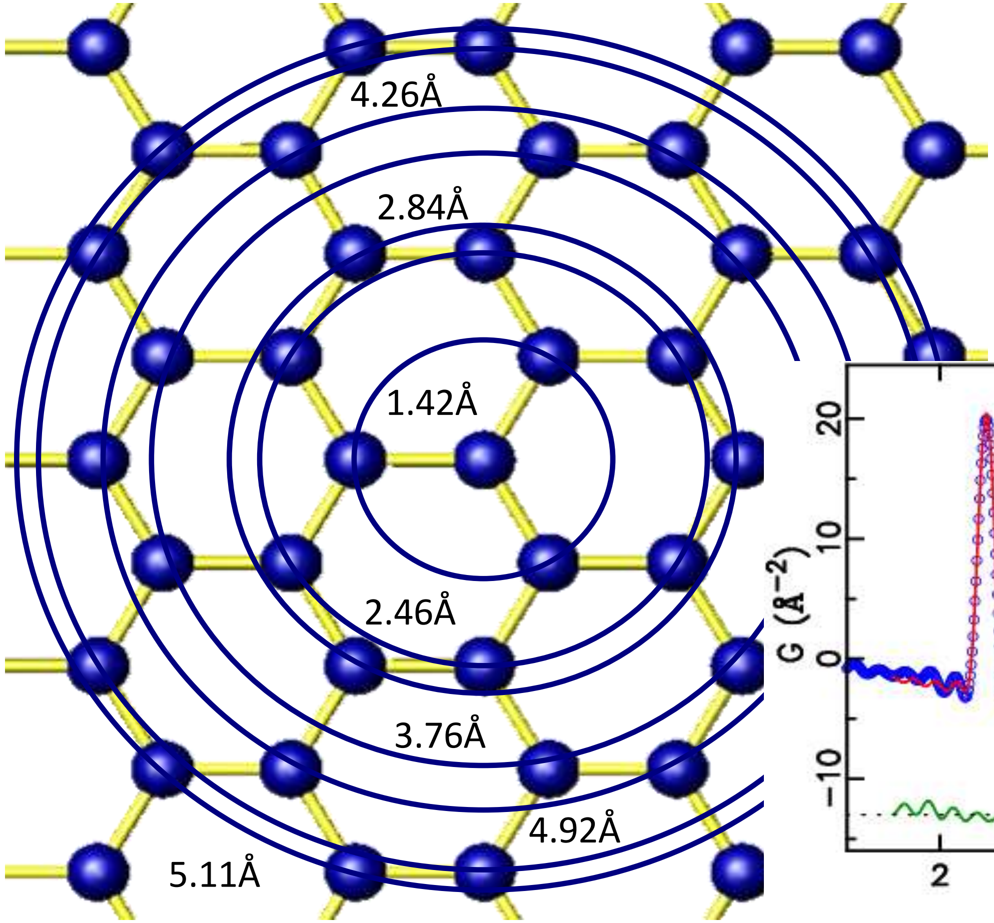

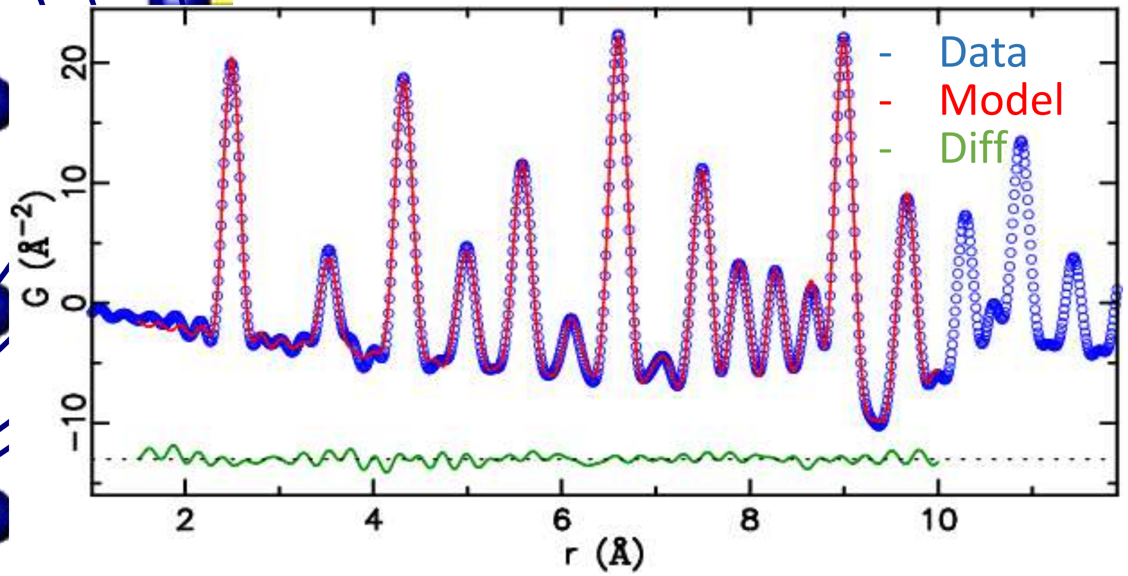

Sub-nanometer resolution

1D-PDF data processing

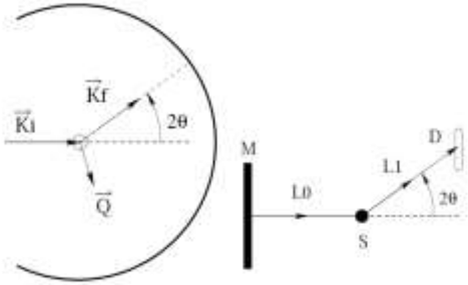

Scattering vector:

$$Q = 4\pi sin(\theta)/\lambda$$

X-ray

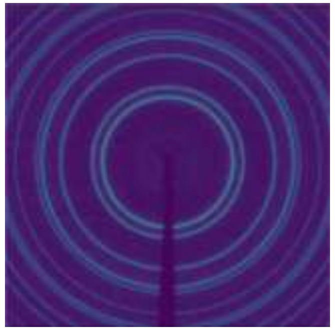

2D Detector

Neutron

TOF Bank Detectors

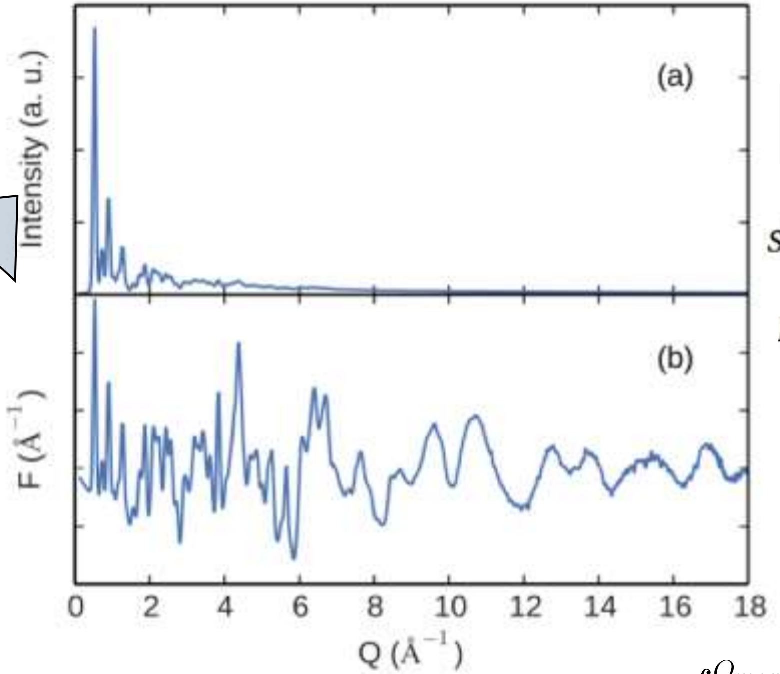

Integrated 1D data

$$S(Q)-1=\frac{I(Q)}{N\langle f\rangle^2}-\frac{\langle f^2\rangle}{\langle f\rangle^2}$$

$$F(Q)=Q[S(Q)-1]$$

Structure function

$$G(r) = (2/\pi)\int_{Q_{min}}^{Q_{max}} F(Q)sin(Qr)dQ$$

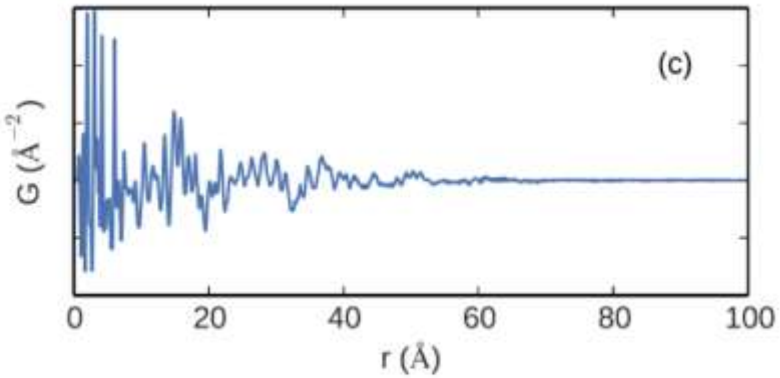

PDF

PDFgetN, PDFgetX

Why do we need spallation neutron source?

- **Low-Q: mostly Bragg peaks.**
- **High-Q: weak diffuse scattering.**

$$Q = \frac{4\pi \sin\theta}{\lambda}$$

- **We need short-wavelength (high-energy), to get large Q_{max}.**
- **To improve real space resolution Δr.**

$$\Delta r \sim \frac{\pi}{Q_{max}}$$

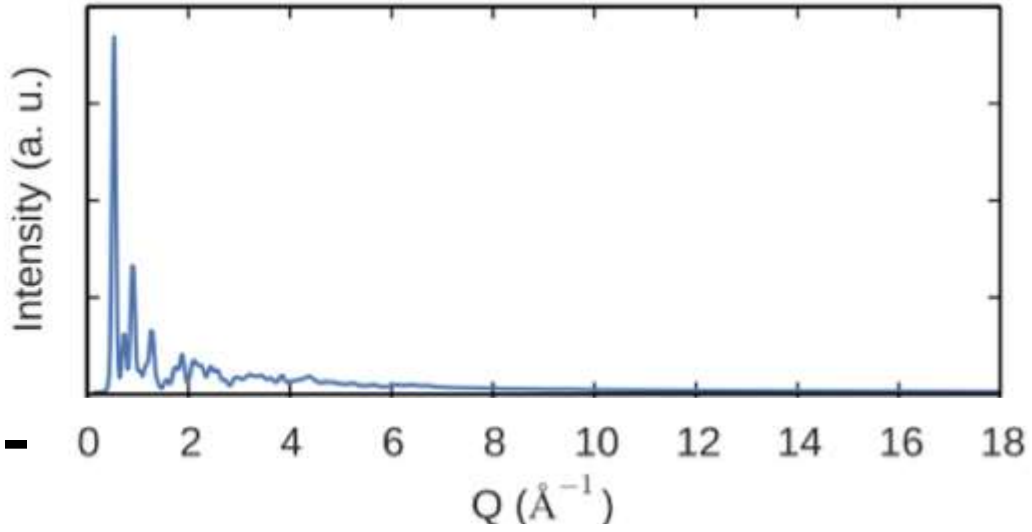

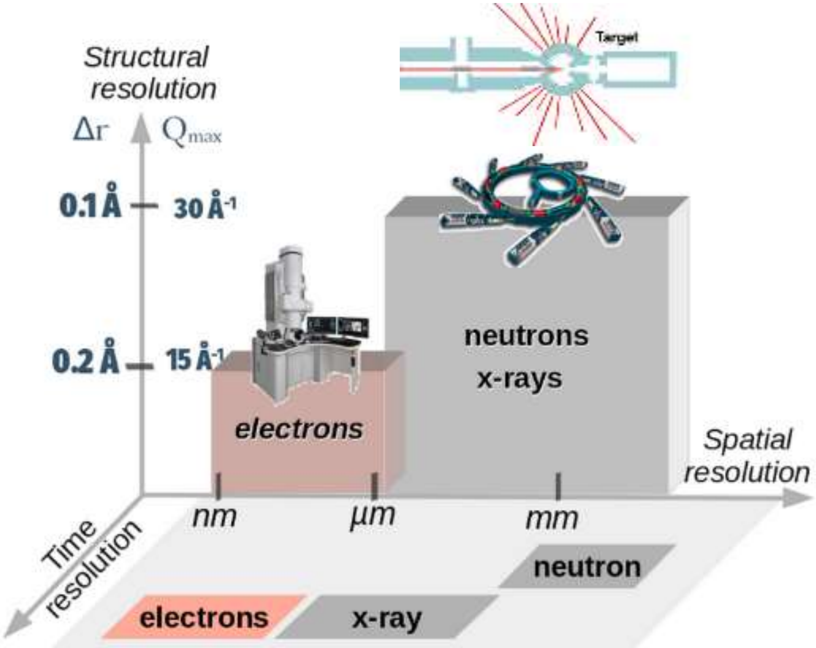

Local structure probe

- In a neutron total scattering experiment, we can obtain both!

Atomic PDF

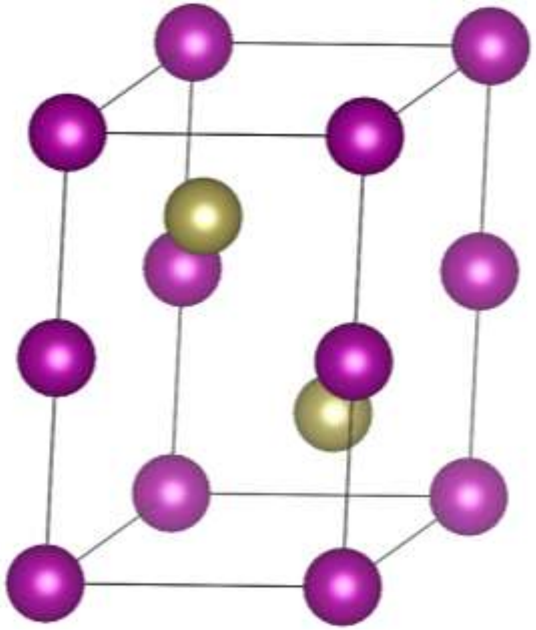

Local atomic structure

Magnetic PDF

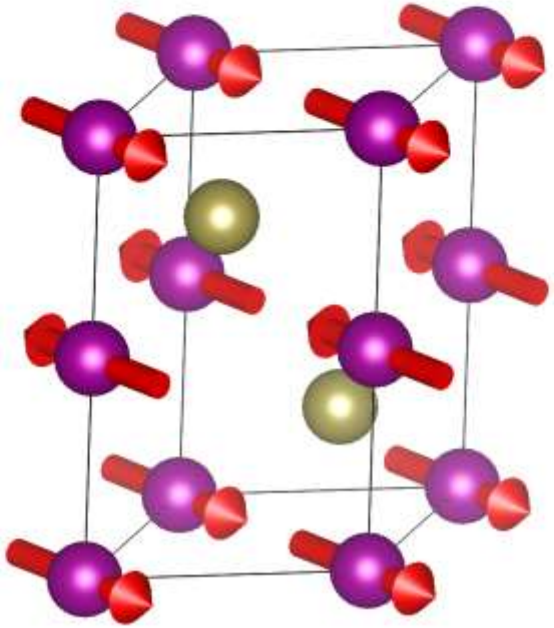

Local magnetic structure

mPDF theory

The orientationally averaged magnetic scattering (Blech and Averbach. Physics, 1964):

$$\frac{\mathrm{d}\sigma}{\mathrm{d}\Omega} = \frac{2}{3} NS(S+1)(\gamma r_0)^2 f^2 + (\gamma r_0)^2 f^2 \times \sum_{i \neq j} \left\{ A_{ij} \frac{\sin \kappa r_{ij}}{\kappa r_{ij}} + B_{ij} \left[\frac{\sin \kappa r_{ij}}{(\kappa r_{ij})^3} - \frac{\cos \kappa r_{ij}}{(\kappa r_{ij})^2} \right] \right\}$$

Self-scattering (i=j)

$$A_{ij} = \left\langle S_i^y S_j^y \right\rangle \qquad B_{ij} = 2\left\langle S_i^x S_j^x \right\rangle - \left\langle S_i^y S_j^y \right\rangle$$

$$S(\kappa) = \frac{\mathrm{d}\sigma/\mathrm{d}\Omega}{\frac{2}{3} N\, S(S+1)(\gamma r_0)^2 f^2} = 1 + \frac{1}{N} \frac{3}{2S(S+1)} \times \sum_{i \neq j} \left\{ A_{ij} \frac{\sin \kappa r_{ij}}{\kappa r_{ij}} + B_{ij} \left[\frac{\sin \kappa r_{ij}}{(\kappa r_{ij})^3} - \frac{\cos \kappa r_{ij}}{(\kappa r_{ij})^2} \right] \right\}$$

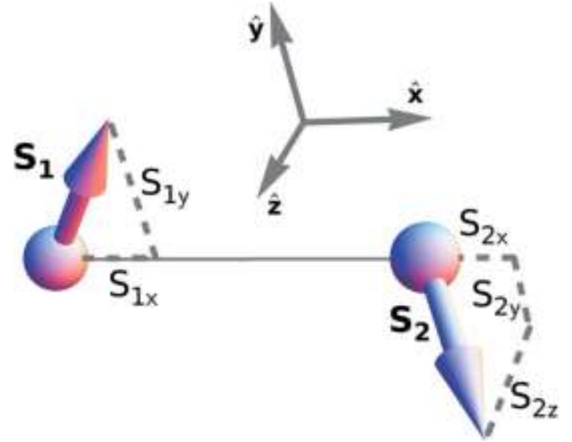

$$\hat{\mathbf{x}} = \frac{\mathbf{r}_j - \mathbf{r}_i}{|\mathbf{r}_j - \mathbf{r}_i|} \text{ and } \hat{\mathbf{y}} = \frac{\mathbf{S}_i - \hat{\mathbf{x}}(\mathbf{S}_i \cdot \hat{\mathbf{x}})}{|\mathbf{S}_i - \hat{\mathbf{x}}(\mathbf{S}_i \cdot \hat{\mathbf{x}})|}$$

B. Frandsen, X. Yang, S. J.L. Billinge, *Acta Cryst. A*, 2014, 70, 1

mPDF theory

- **Reduced structure function** $F(\kappa) = \kappa[S(\kappa) - 1]$

$$F(\kappa) = \frac{1}{N}\frac{3}{2S(S+1)} \times \sum_{i\neq j}\left[A_{ij}\frac{\sin \kappa r_{ij}}{r_{ij}} + B_{ij}\left(\frac{\sin \kappa r_{ij}}{\kappa^2 r_{ij}^3} - \frac{\cos \kappa r_{ij}}{\kappa r_{ij}^2}\right)\right]$$

- **mPDF via Fourier transform**

$$f(r) = \frac{2}{\pi}\int_0^\infty \mathrm{d}\kappa F(\kappa)\sin \kappa r$$

mPDF contains both spatial and orientational magnetic correlations.

$$= \frac{1}{N}\frac{3}{2S(S+1)}\sum_{i\neq j}\left\{\frac{A_{ij}}{r}\delta(r - r_{ij}) + B_{ij}\frac{r}{r_{ij}^3}[1 - \Theta(r - r_{ij})]\right\}$$

- **Atomic PDF**

$$f_{\mathrm{atPDF}}(r) = (1/rN)\sum_{i\neq j}\delta(r - r_{ij})$$

mPDF theory

$$f(r) = \frac{2}{\pi}\int_0^\infty Q\left[\frac{I_m}{\frac{2}{3}N_s S(S+1)(\gamma r_0)^2 f_m^2(Q)} - 1\right]\sin Qr\,dQ \quad (1)$$

← **Experimental mPDF**

$$= \frac{1}{N_s}\frac{3}{2S(S+1)}\sum_{i\neq j}\left[\frac{A_{ij}}{r}\delta(r-r_{ij}) + B_{ij}\frac{r}{r_{ij}^3}\Theta(r_{ij}-r)\right], \quad (2)$$

← **Simulated mPDF**

- **$f_m(Q)$ is the magnetic form factor**

X-ray	$F_{hkl} = \sum f_j \exp(2\pi i(hx+ky+lz))e^{-2W}$
Neutron	$F_{hkl} = \sum b_j \exp(2\pi i(hx+ky+lz))e^{-2W}$
Magnetic	$F_{hkl} = \sum q_j f_{Mj} \exp(2\pi i(hx+ky+lz))e^{-2W}$

mPDF

Ferromagnetic

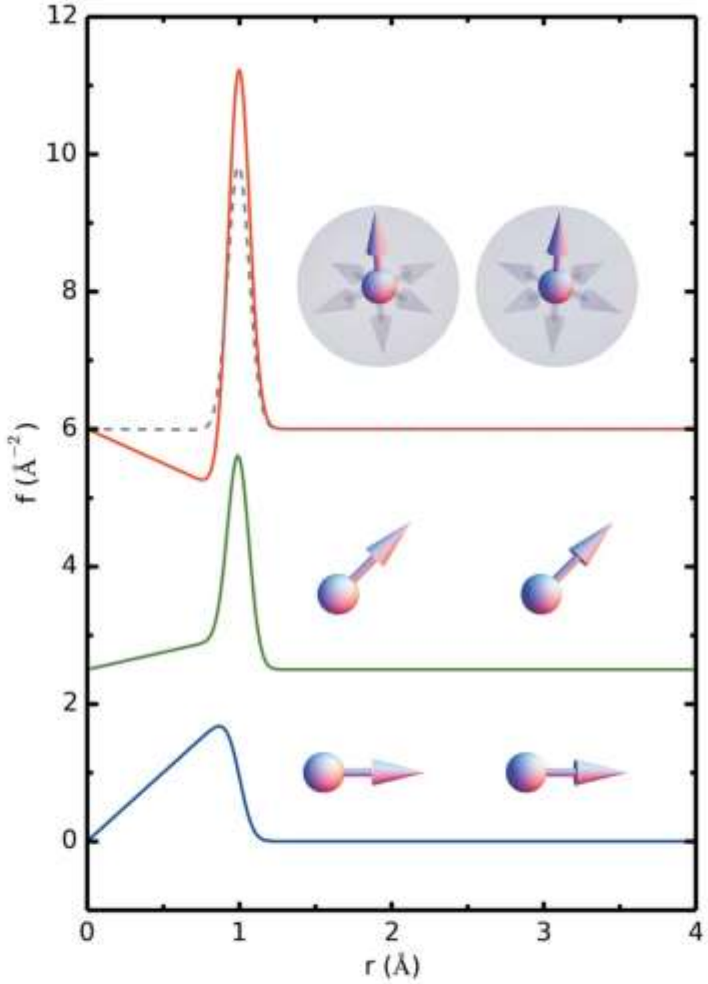

Positive peak

Antiferromagnetic

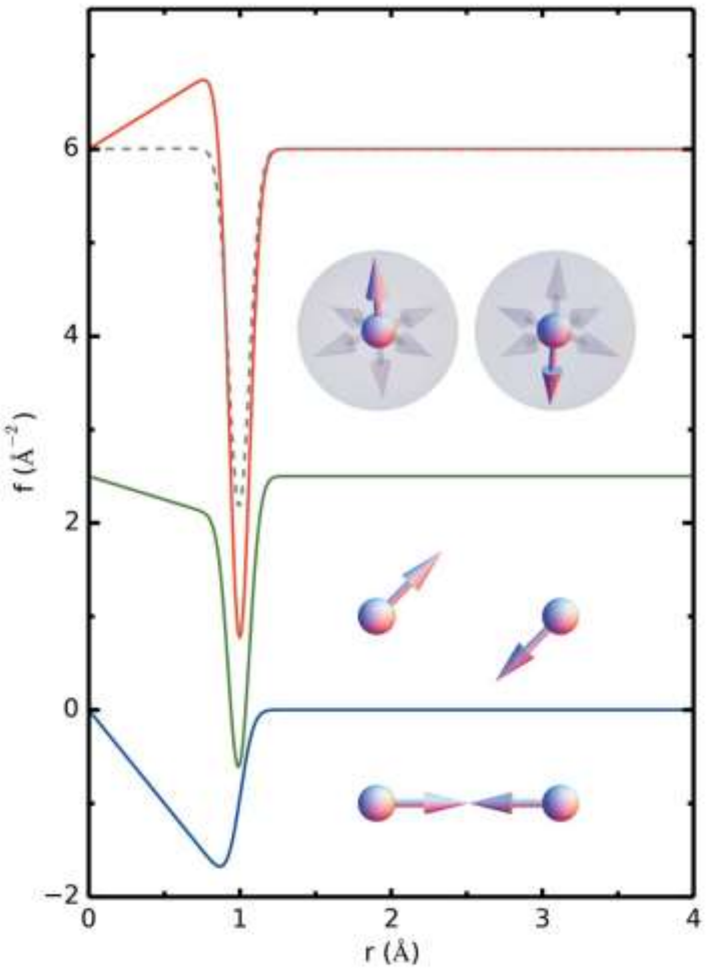

Negative peak

mPDF

1D structure

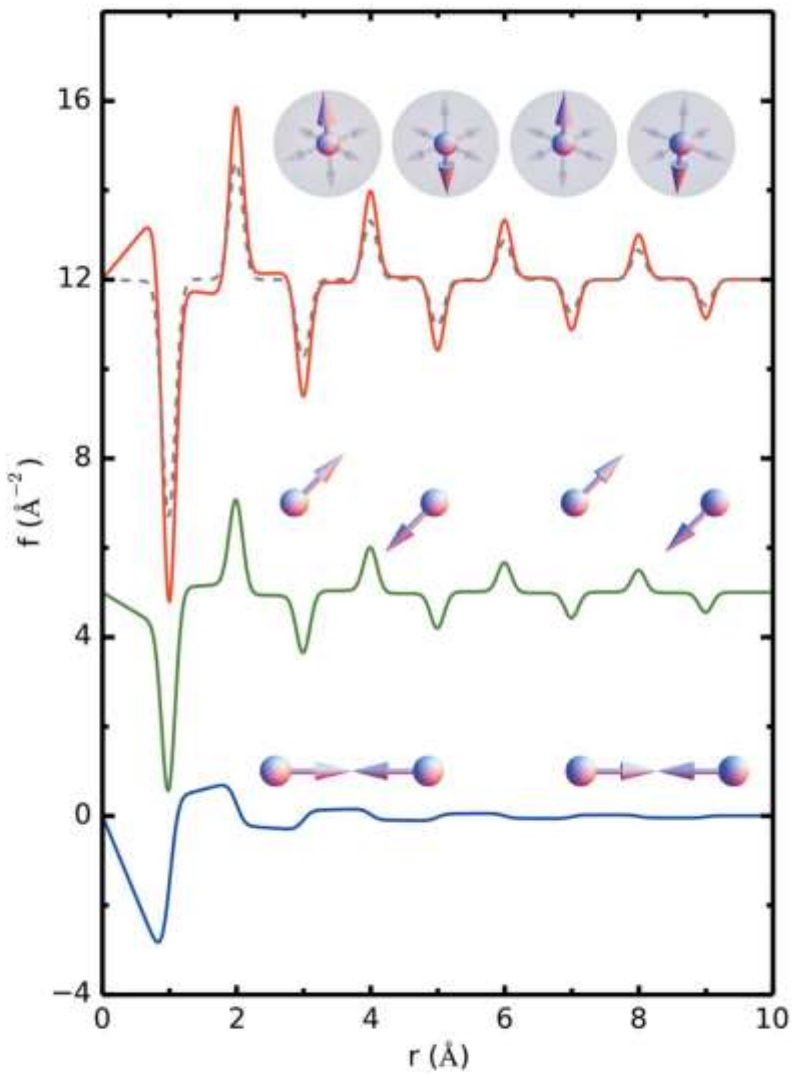

3D structure

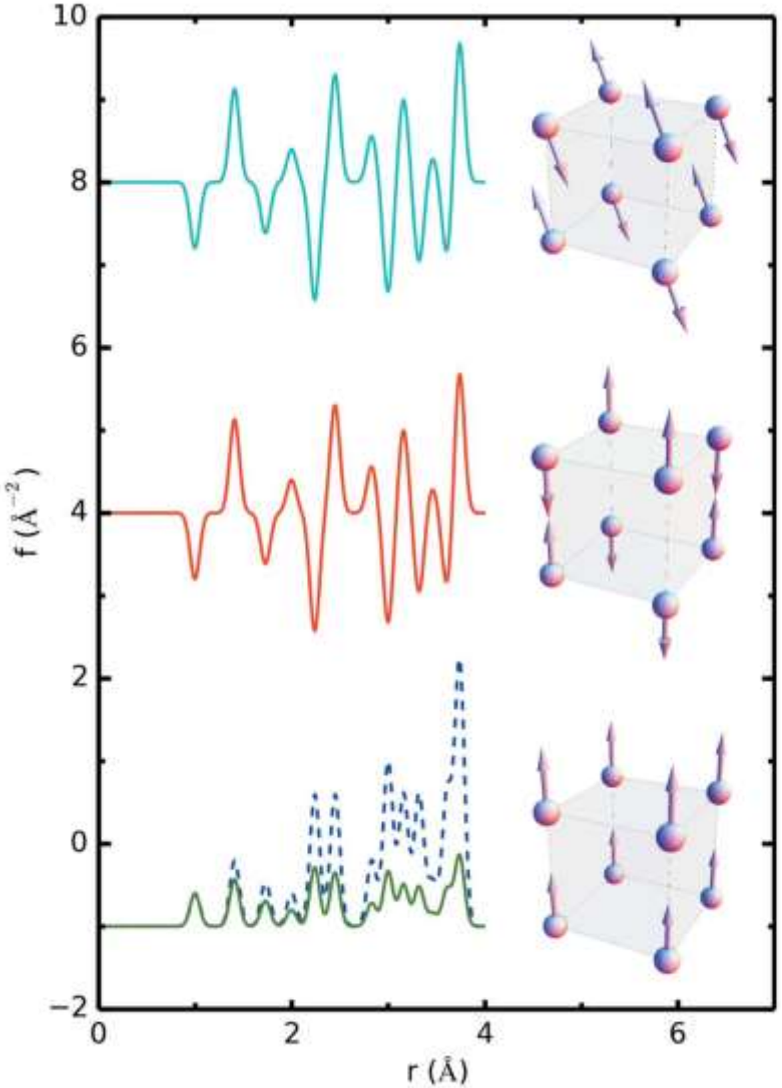

DiffPy.mPDF

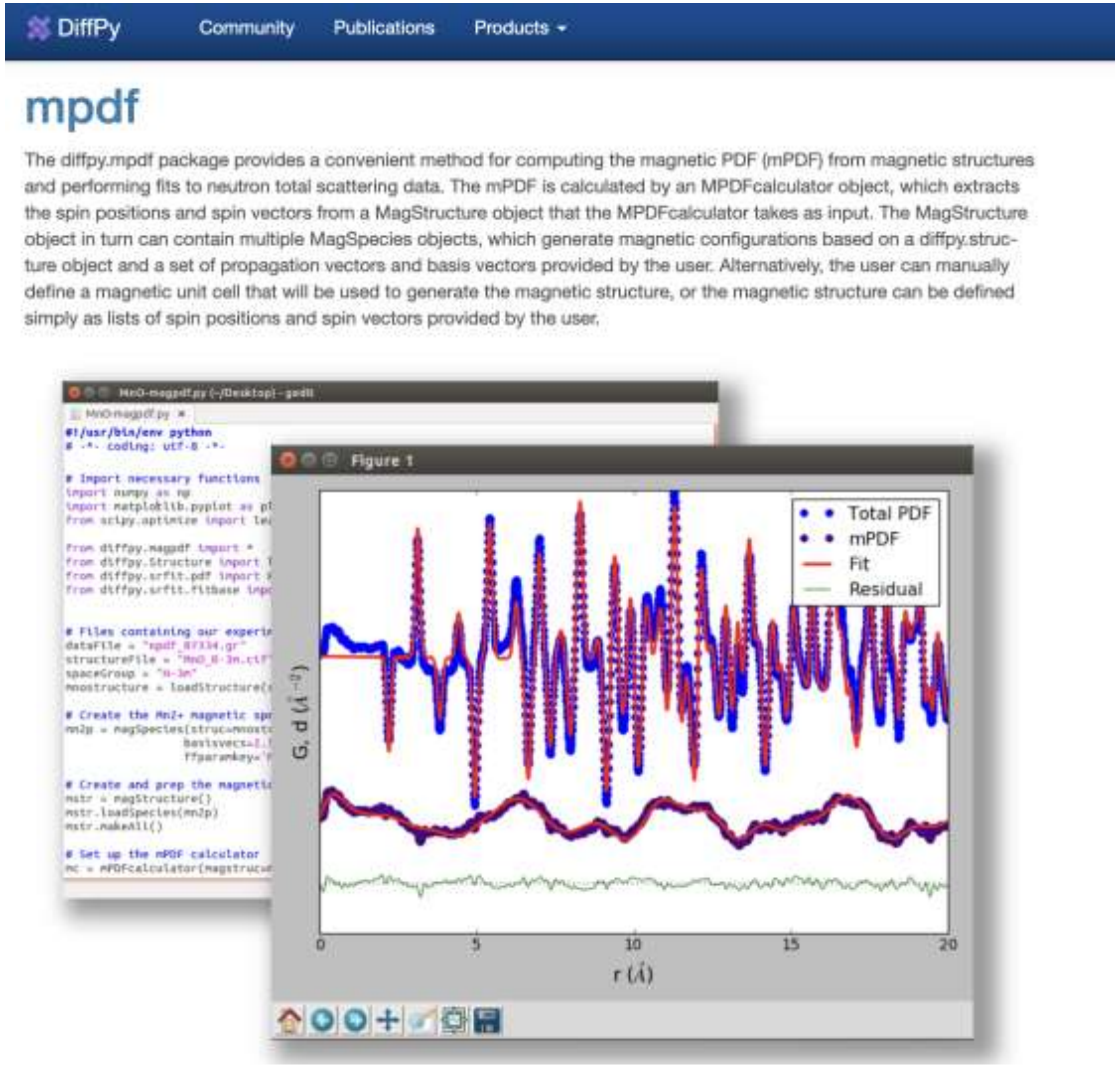

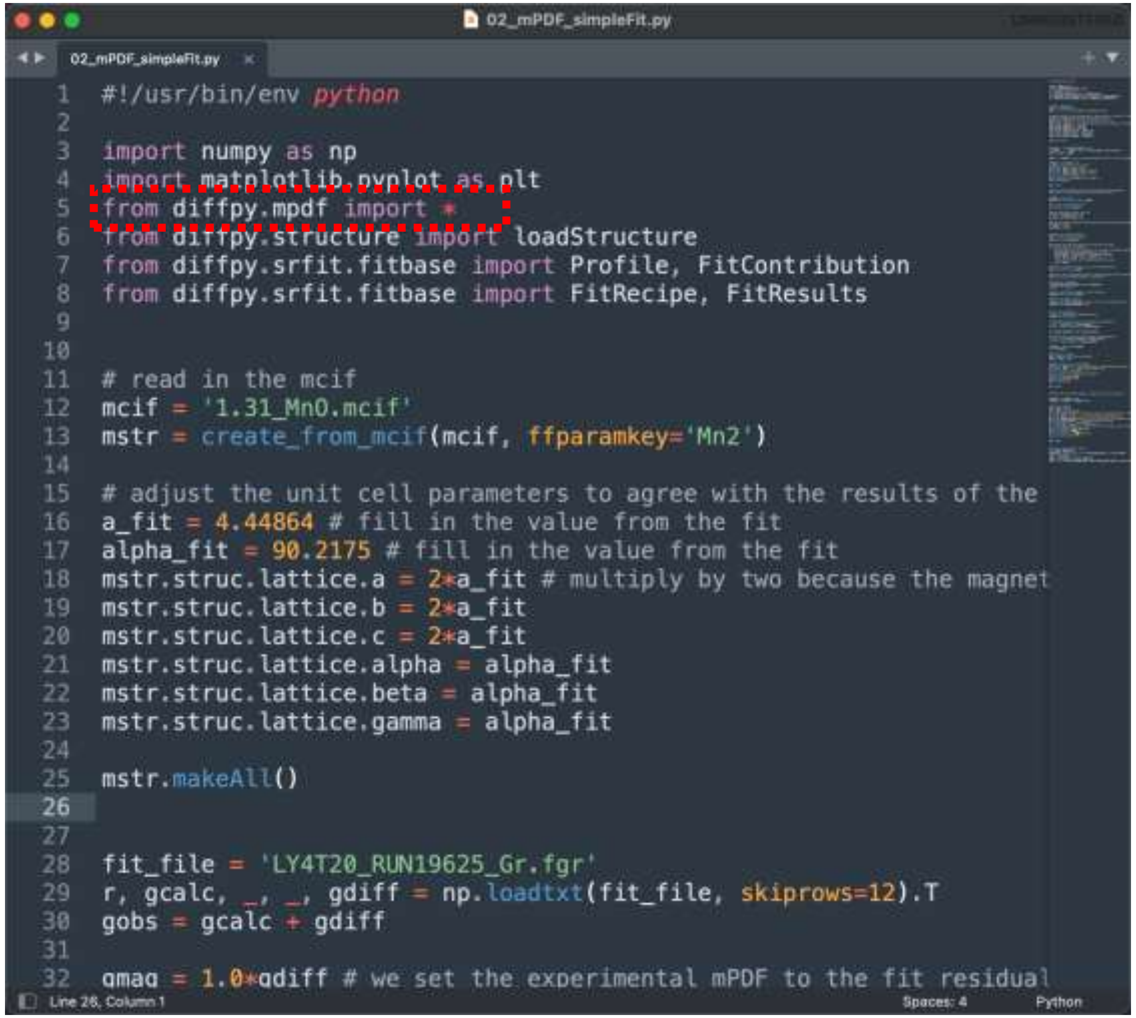

https://www.diffpy.org/products/mPDF.html

DiffPy.mPDF

Normalized v.s. Unnormalized

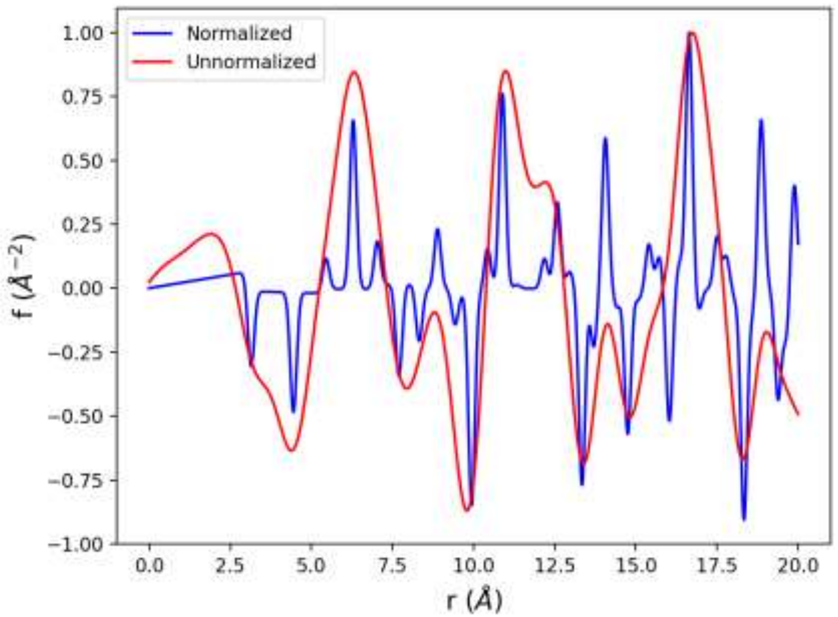

Q_{max} effect

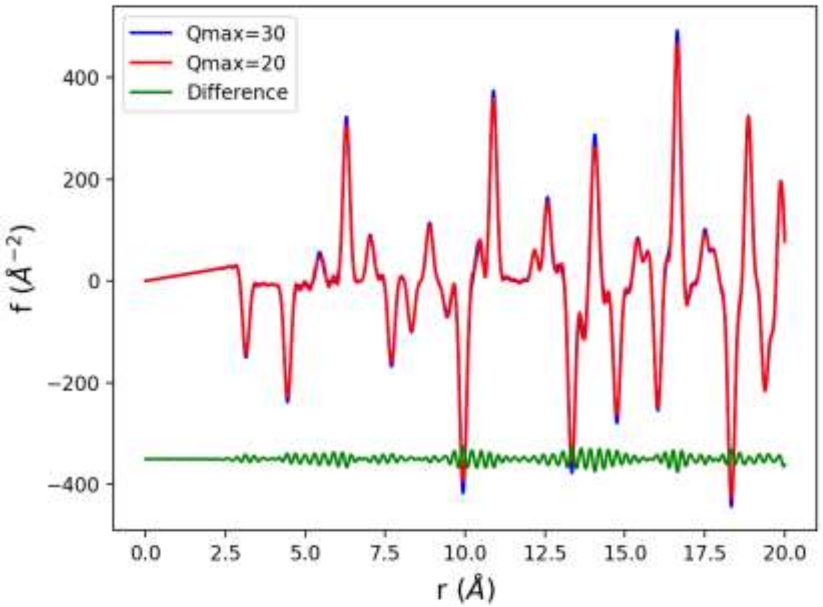

Finite correlation length

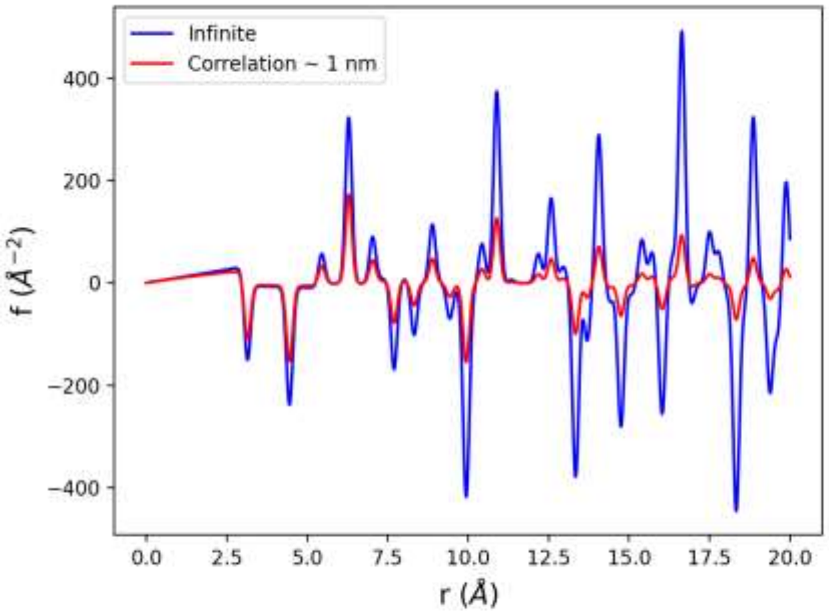

DiffPy.mPDF

Different spin directions

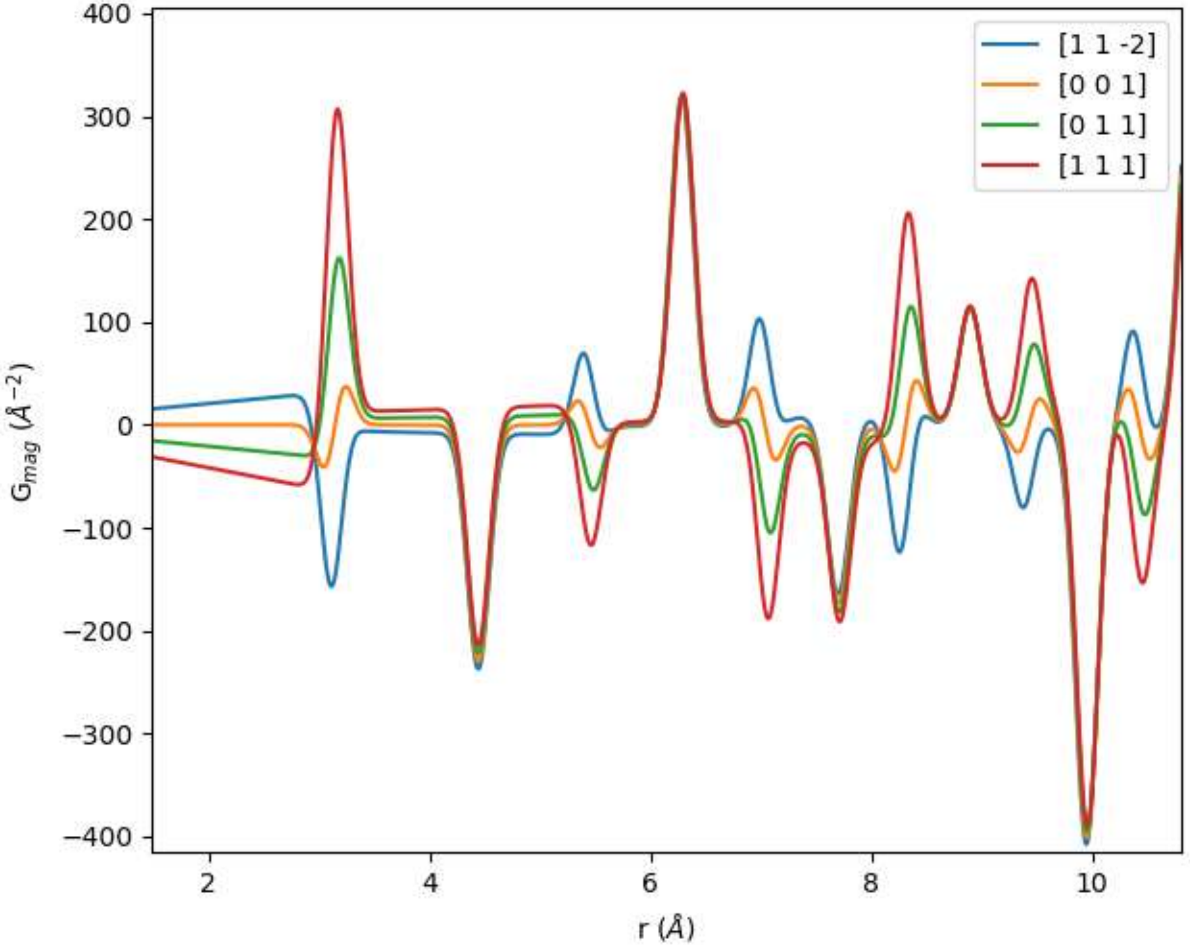

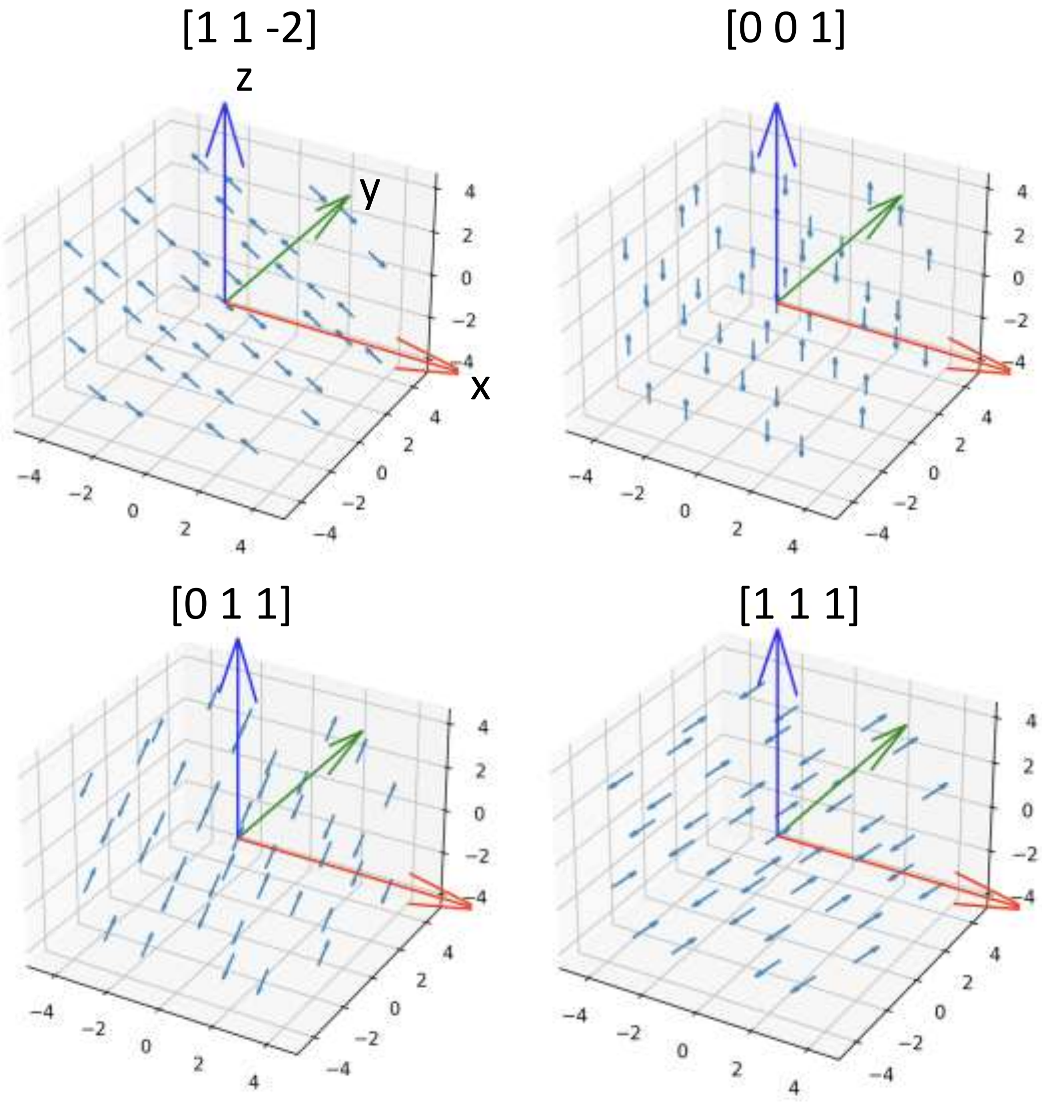

Multi-physics instrument, CSNS

- **The first total scattering neutron diffractometer in China.**

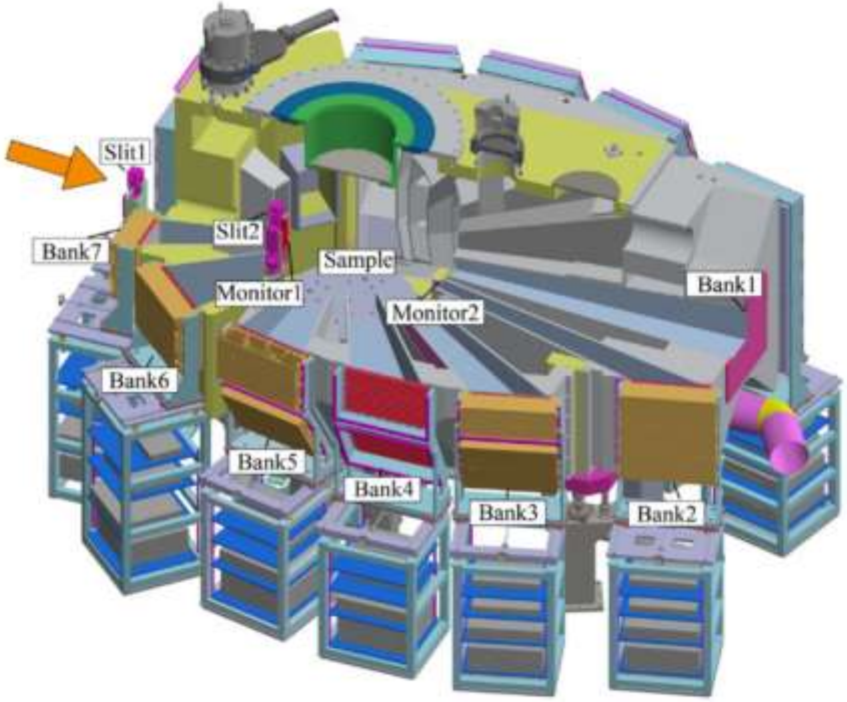

Nuclear Inst. and Methods in Physics Research, A 1013 (2021) 165642

Contents lists available at ScienceDirect

Nuclear Inst. and Methods in Physics Research, A

journal homepage: www.elsevier.com/locate/nima

Multi-physics instrument: Total scattering neutron time-of-flight diffractometer at China Spallation Neutron Source

Juping Xu [a,b], Yuanguang Xia [a,b], Zhiduo Li [a,b], Huaican Chen [a,b], Xunli Wang [d], Zhenzhong Sun [c], Wen Yin [a,b,*]

[a] Institute of High Energy Physics, Chinese Academy of Sciences (CAS), Beijing 100049, China
[b] Spallation Neutron Source Science Center (SNSSC), Dongguan 523803, China
[c] School of Mechanical Engineering, Dongguan University of Technology, Dongguan 523803, China
[d] Department of Physics and Materials Science, City University of Hong Kong, 83 Tat Chee Avenue, Kowloon, Hong Kong, China

Table 1
Parameters of the MPI detector array.

Detector bank No.	Secondary flight path *L2* (m)	Scattering angle *2θ* (Degree)	^{3}He tube style	Number of ^{3}He tubes/ modules [a]	Number of ^{3}He tubes/ modules [a]	Calculated dQ/Q @~1 Å	Estimated Q range (Å^{-1})
Bank01	2.82	2.9–5.04	0.5 m×1/2 inch	–	20/1	–	0.1-2.7
Bank02	2.319–2.711	12.54–17.62	Type-1:20 atm, 0.5 m×1 inch	–	96/12	6%	0.45-9
Bank03	1.772–2.065	31-42.25		32/4	96/12	2.1%	1.1-22
Bank04	1.351–1.599	51.25–67.32		48/6	112/14	1.3%	1.8-34
Bank05	1..131-1.220	81.55–105.18		72/9	112/14	0.8%	2.7-49
Bank06	1.166–1.191	121.80–145.51		32/4	64/8	0.55%	3.6-59
Bank07	1.232–1.314	157.47–170.00	Type-2: 20 atm, 0.3 m× 1 inch	64/8	64/8	0.39%	4.1-62

MnO data

20 K

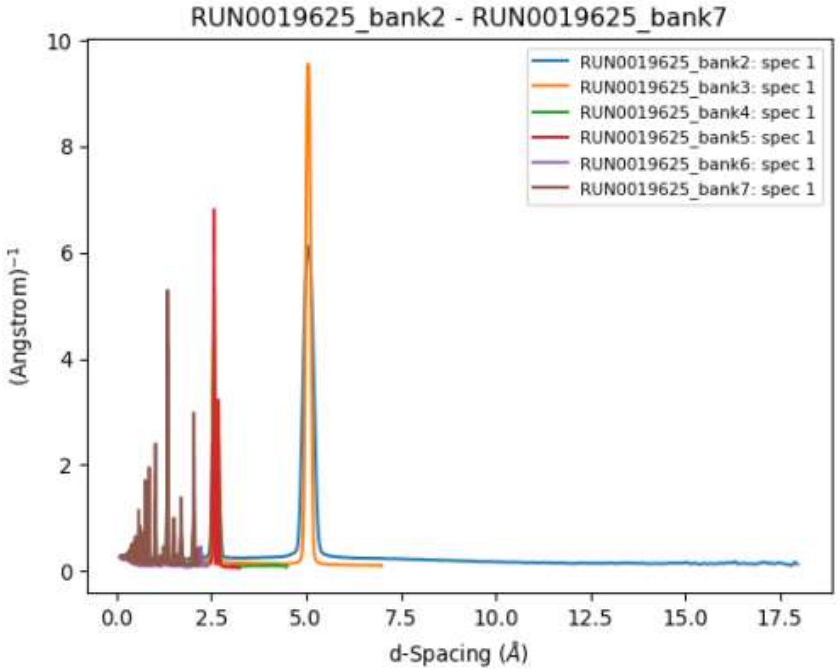

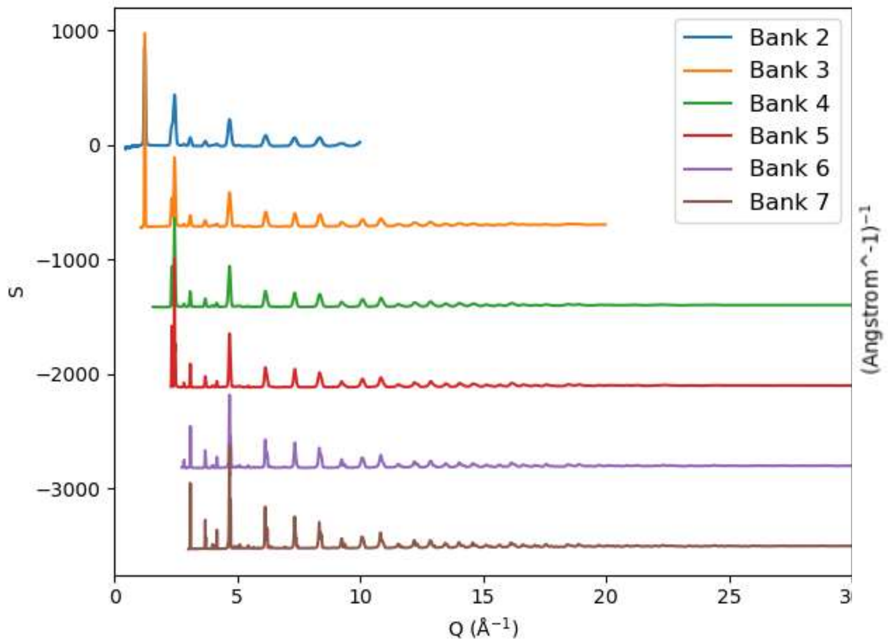

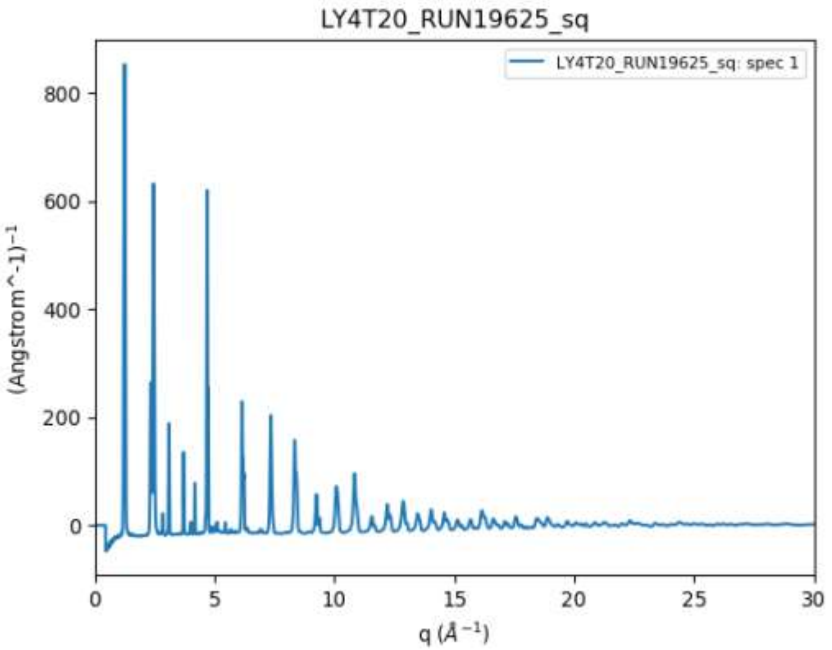

Experiment setup

- **Sample Environment: CCR06**
- **Sample holder: 9mm vanadium can**
- **Sample install: He glovebox**
- **Sealed ring: In**
- **Neutron wavelength: 0.1-4.5Å**

Data collected at March 2023 @ MPI

Courtesy of Juping Xu (CSNS)

PDF

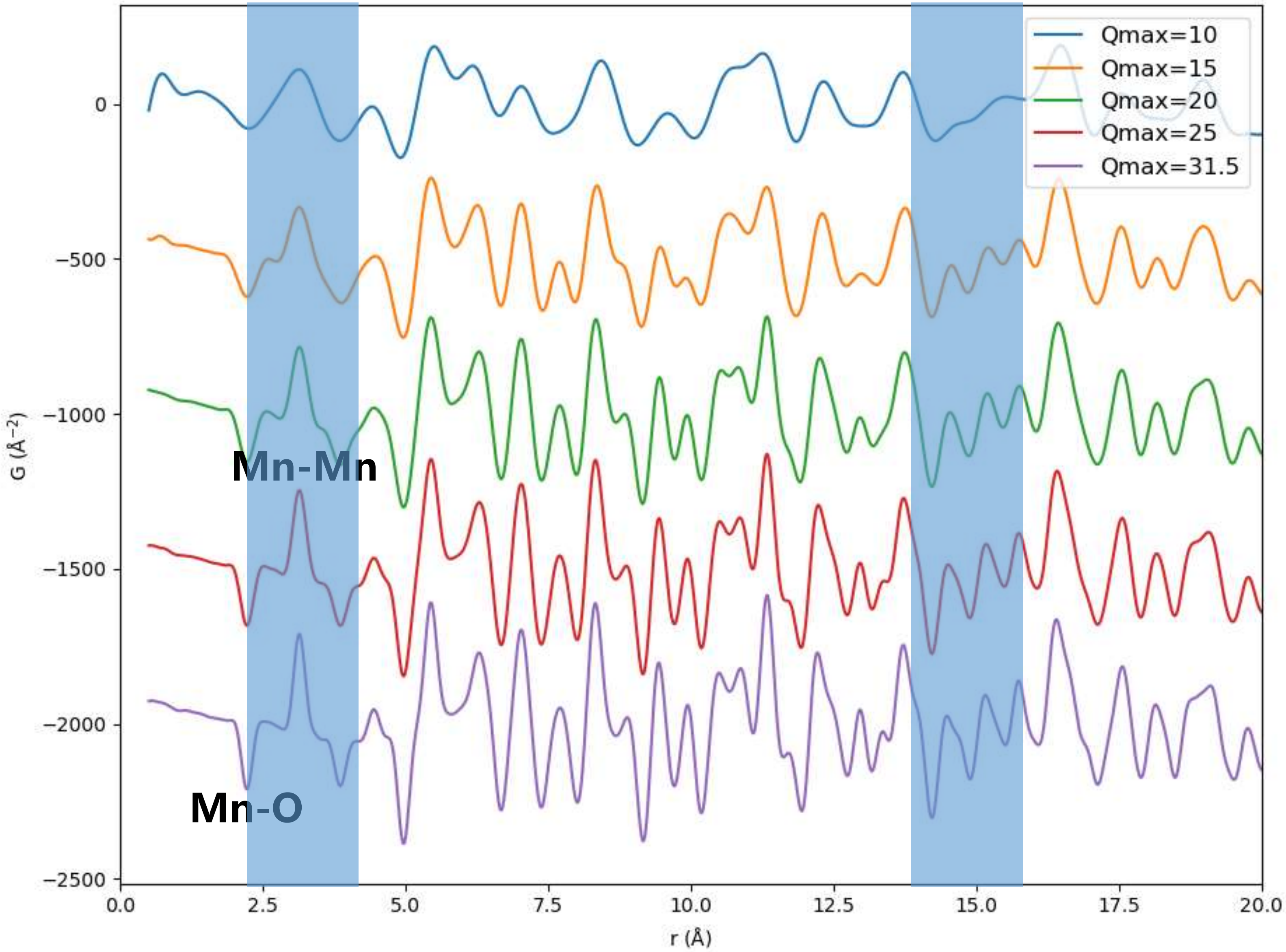

Q_{max}=10 $Å^{-1}$

Q_{max}=20 $Å^{-1}$

Q_{max}=31.5 $Å^{-1}$

MnO data

300 K

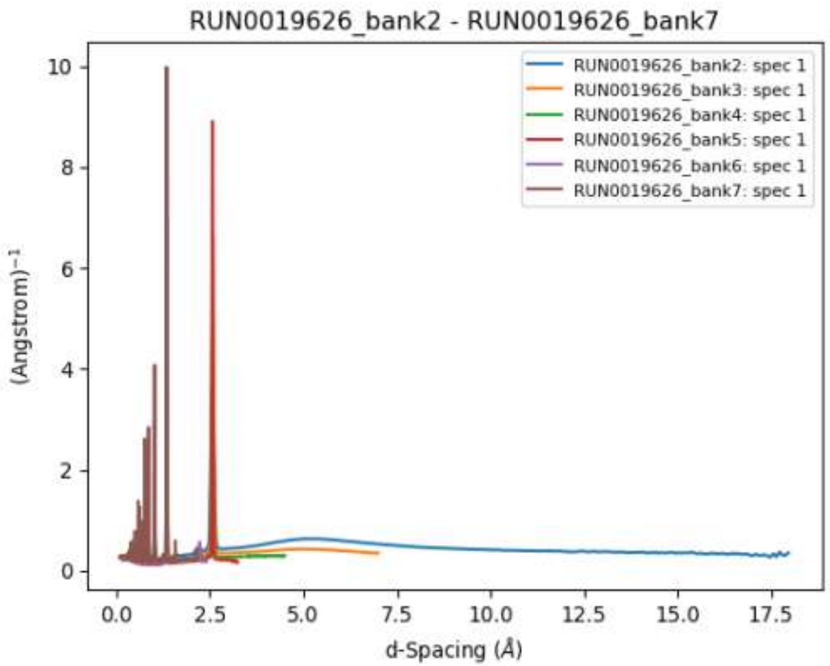

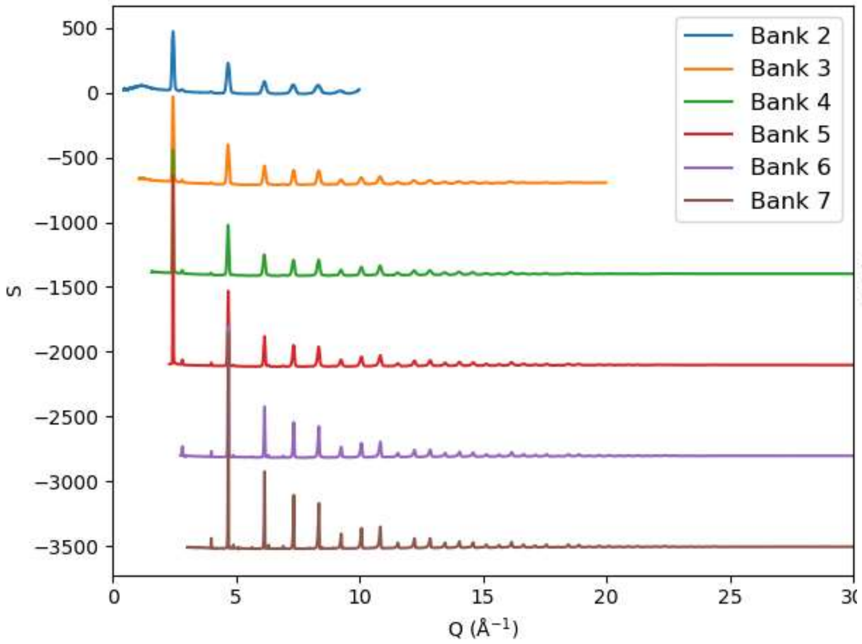

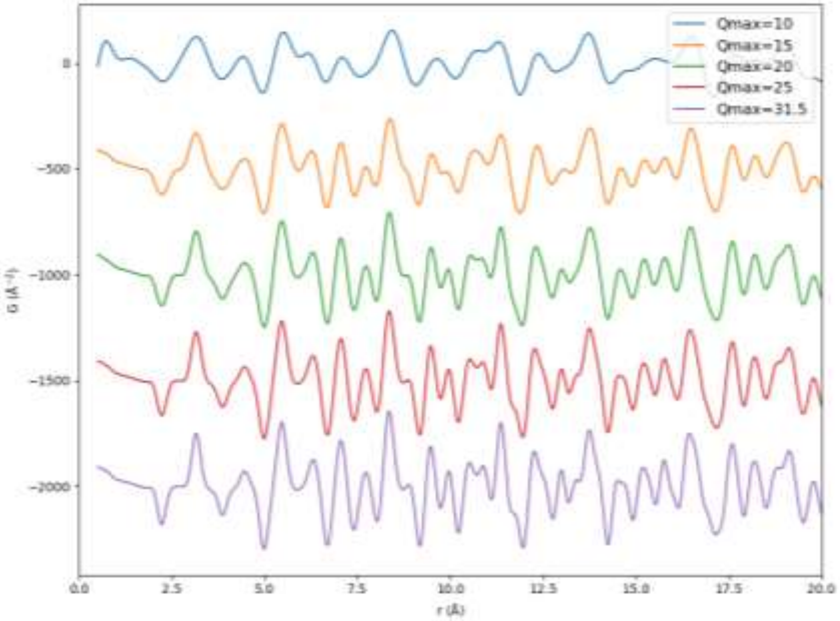

Reciprocal space data analysis

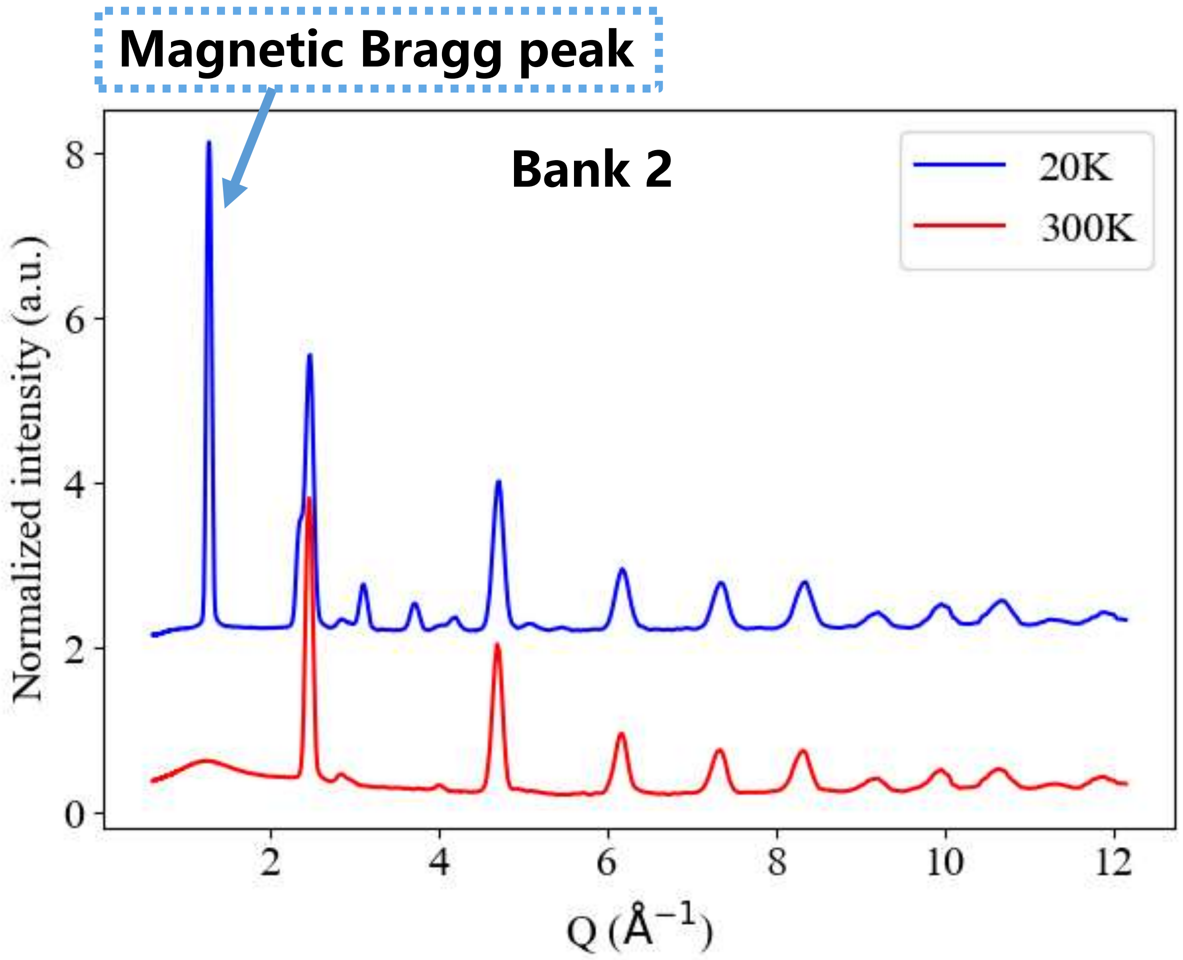

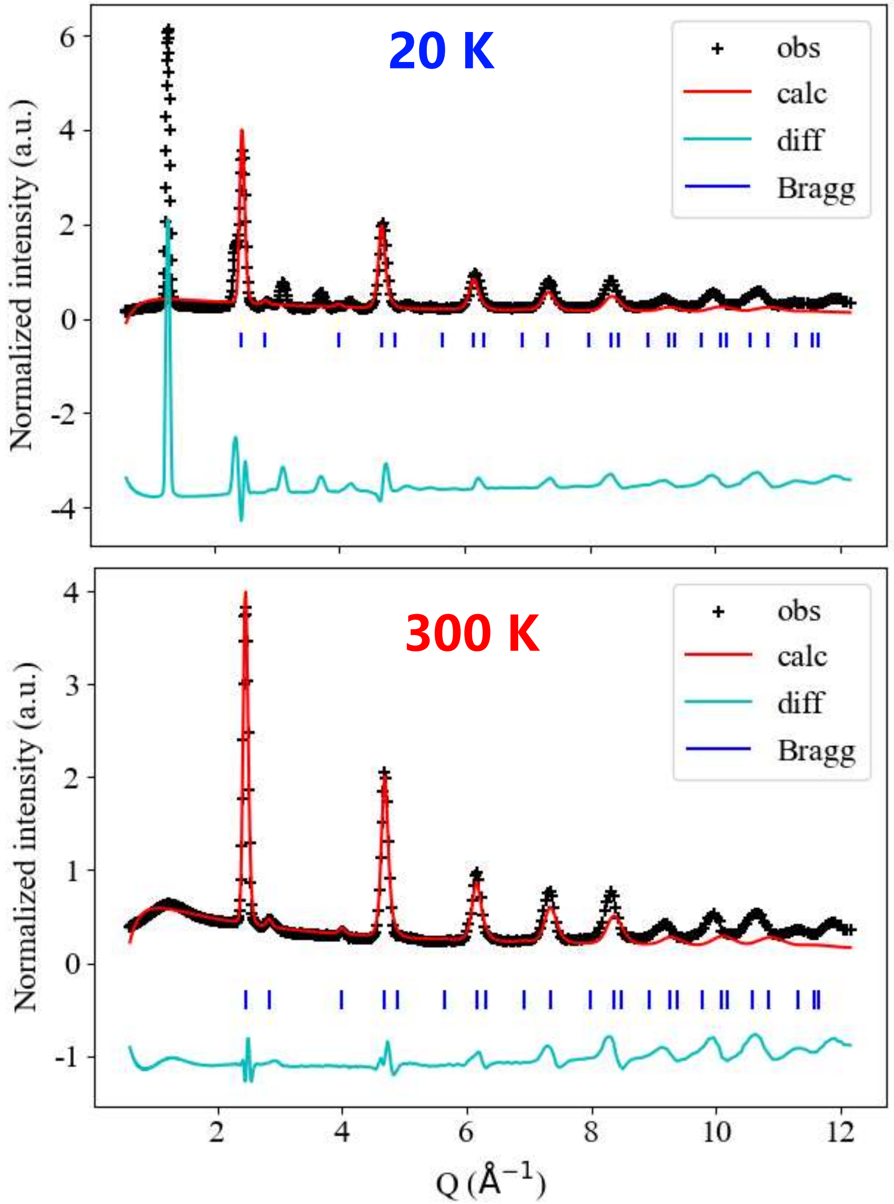

Real space atomic PDF data analysis

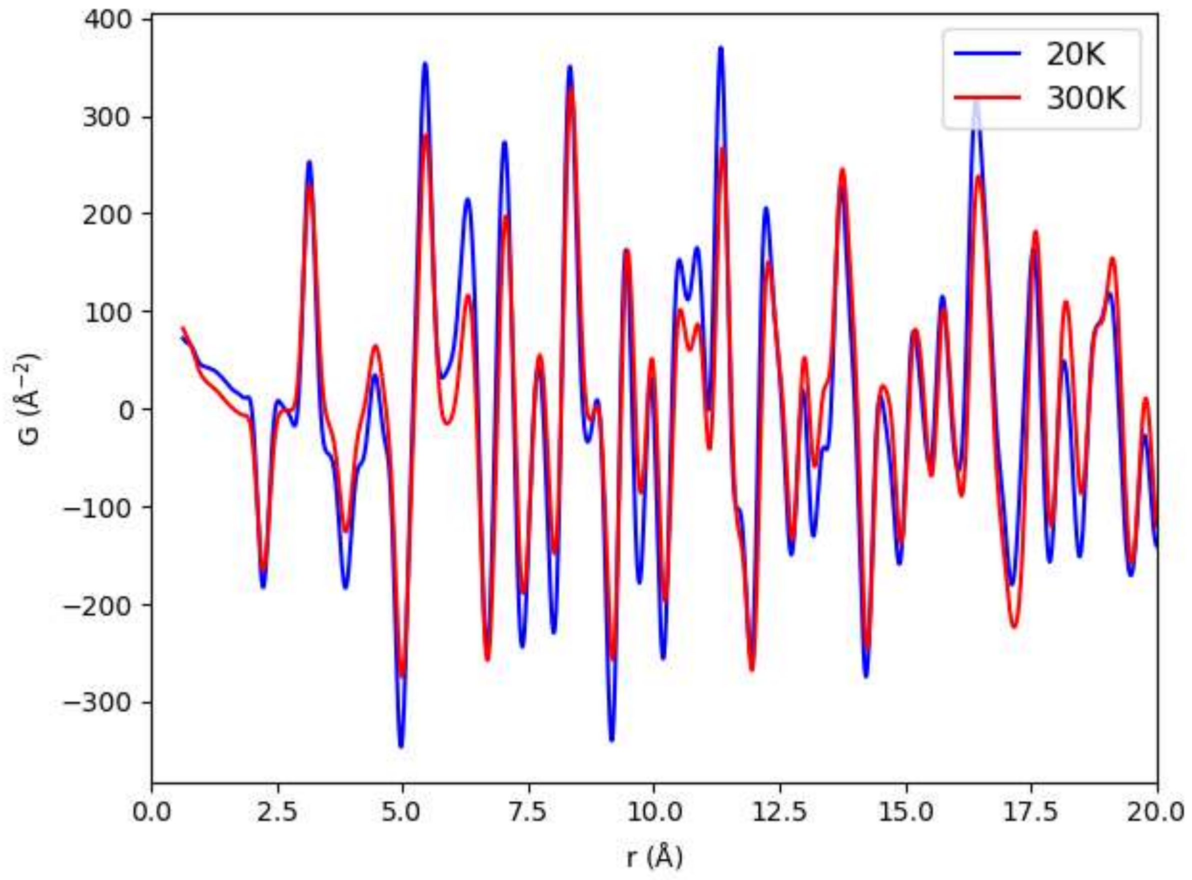

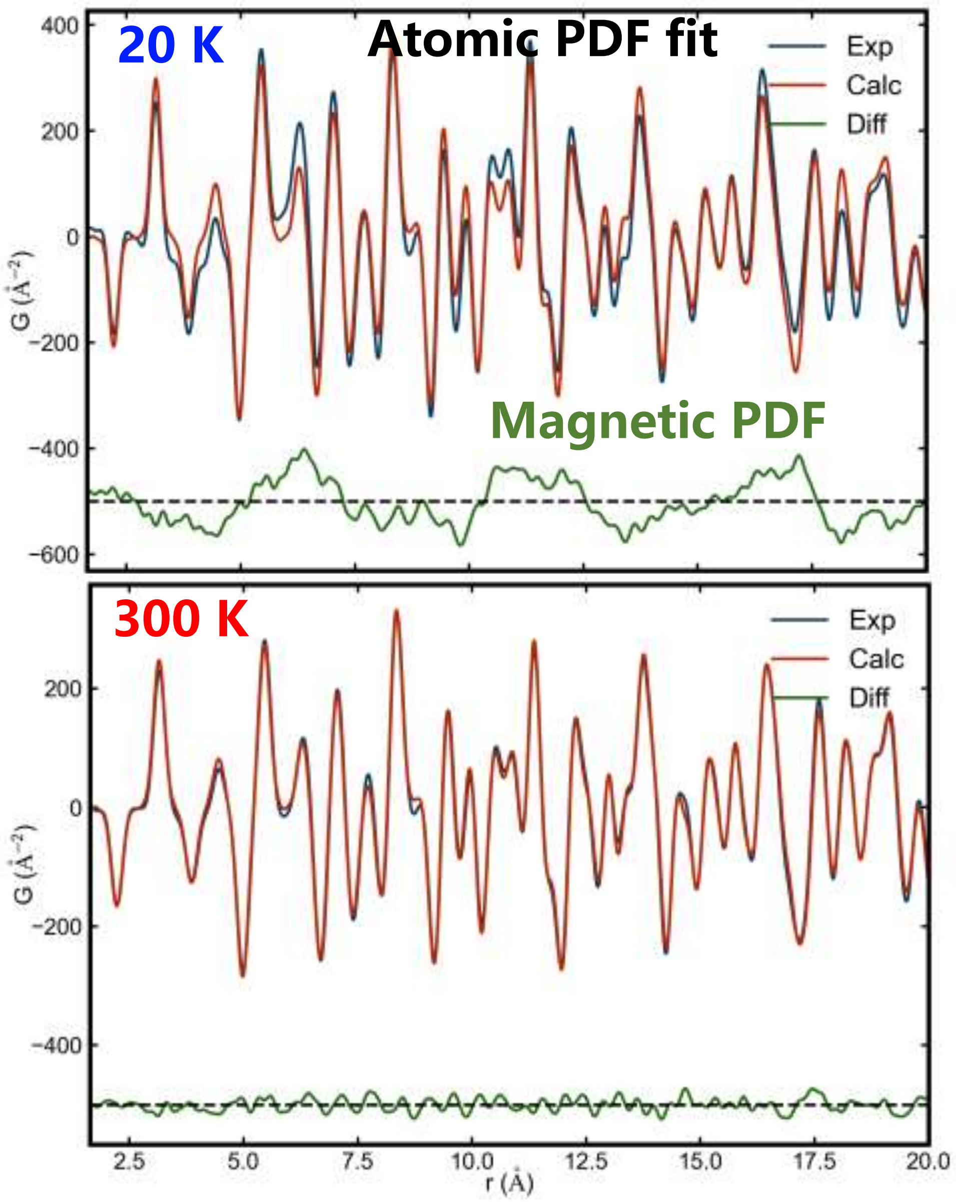

- **After fitting atomic structure, the magnetic signals left are prominent.**

Software framework

Co-Refinement Mode

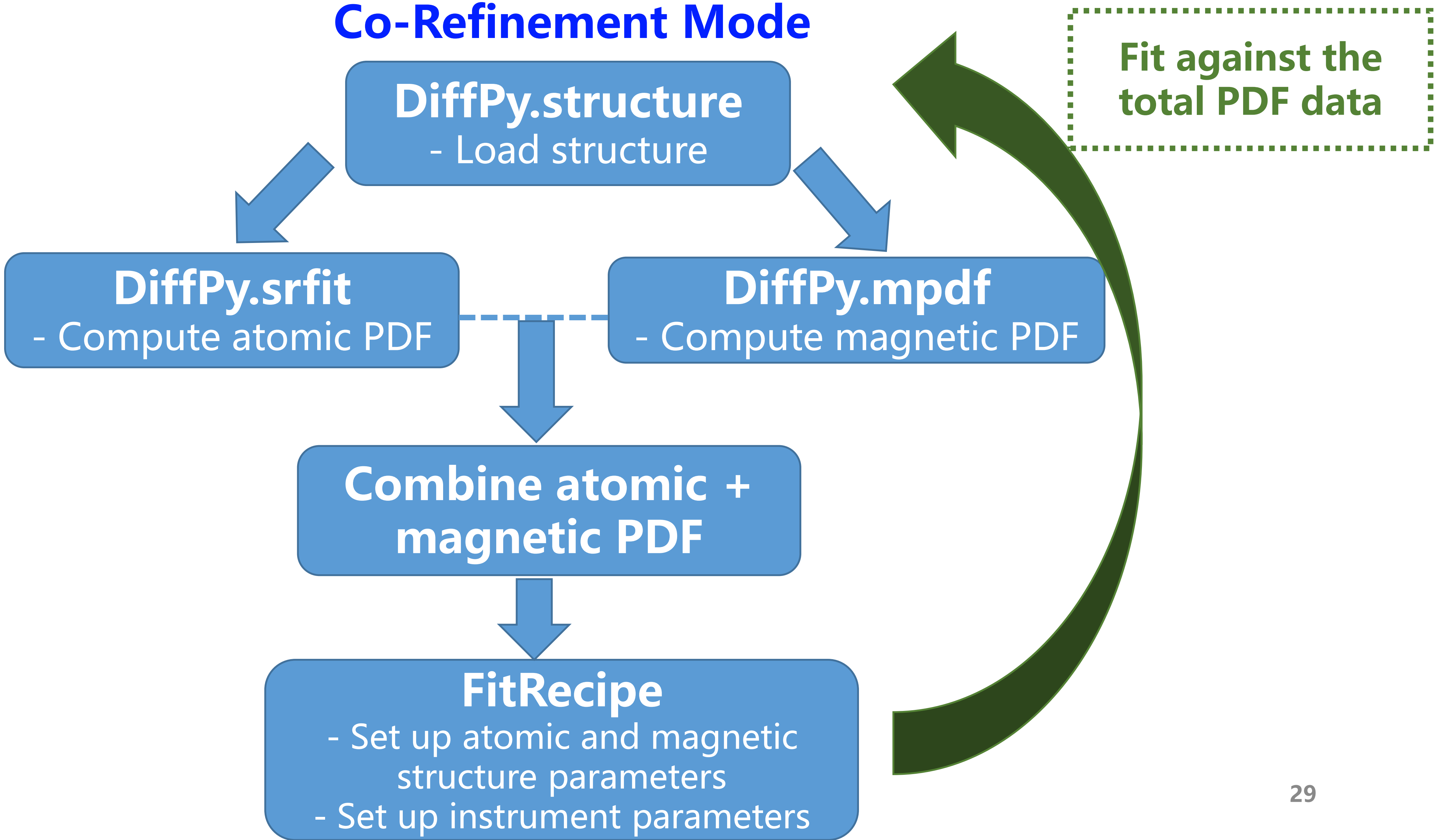

Software framework

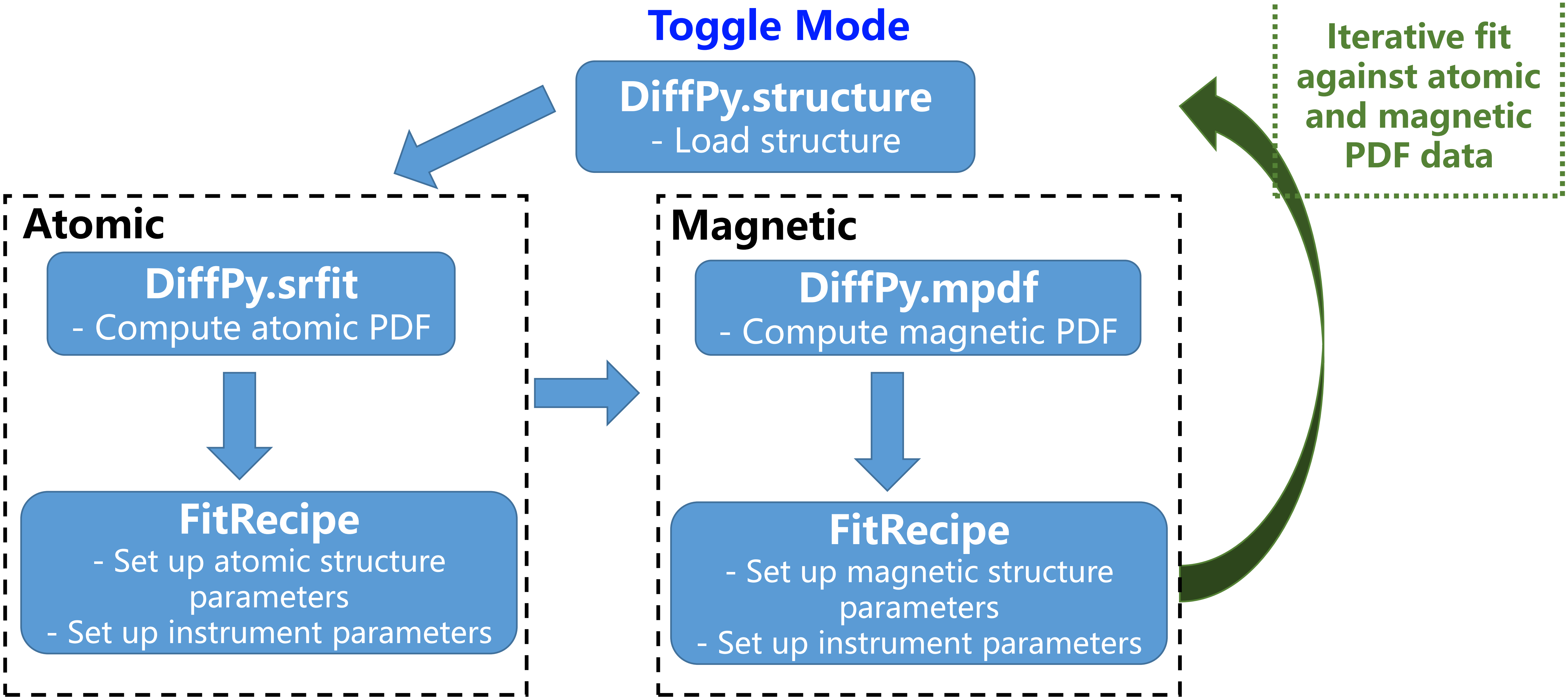

Magnetic structure

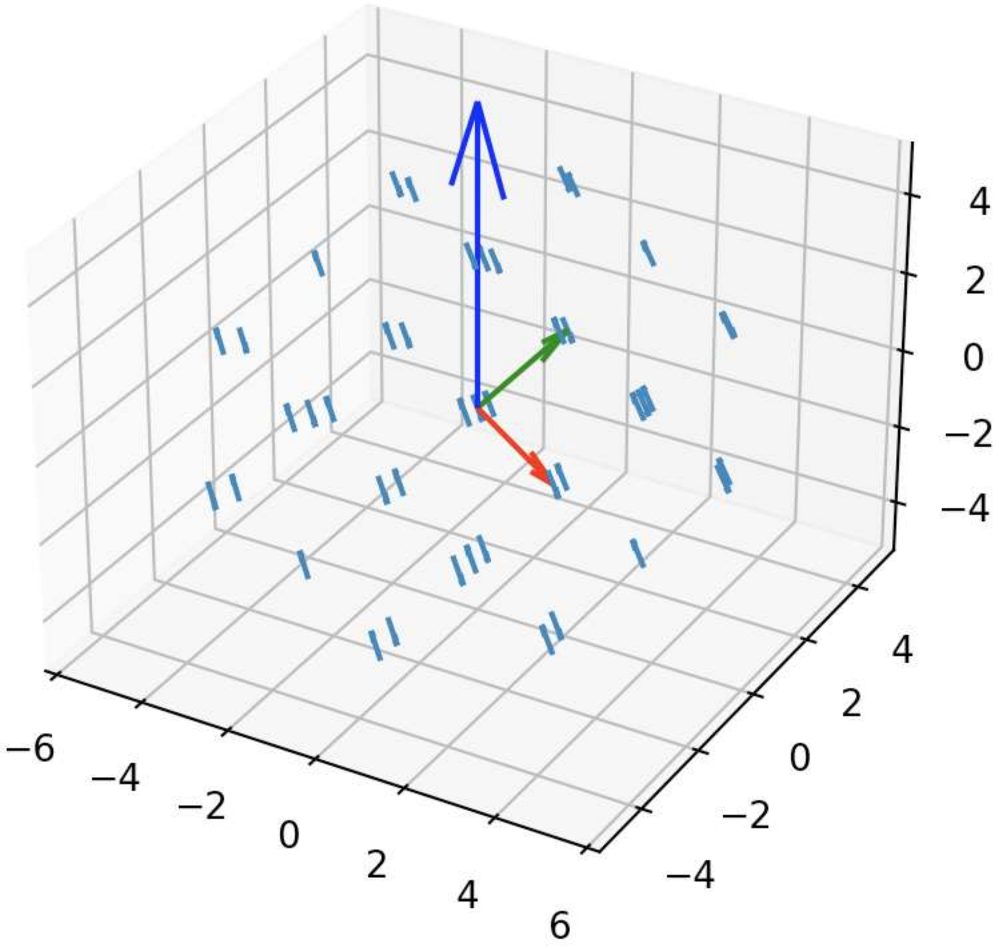

Set up initial magnetic structure

- **Magnetic basis vector = [1, -1, 0]**
- **Magnetic propagation vector = [0, 0, 1.5]**

Q_{max}=25 Å^{-1}

Co-refinement

R_w = 0.086

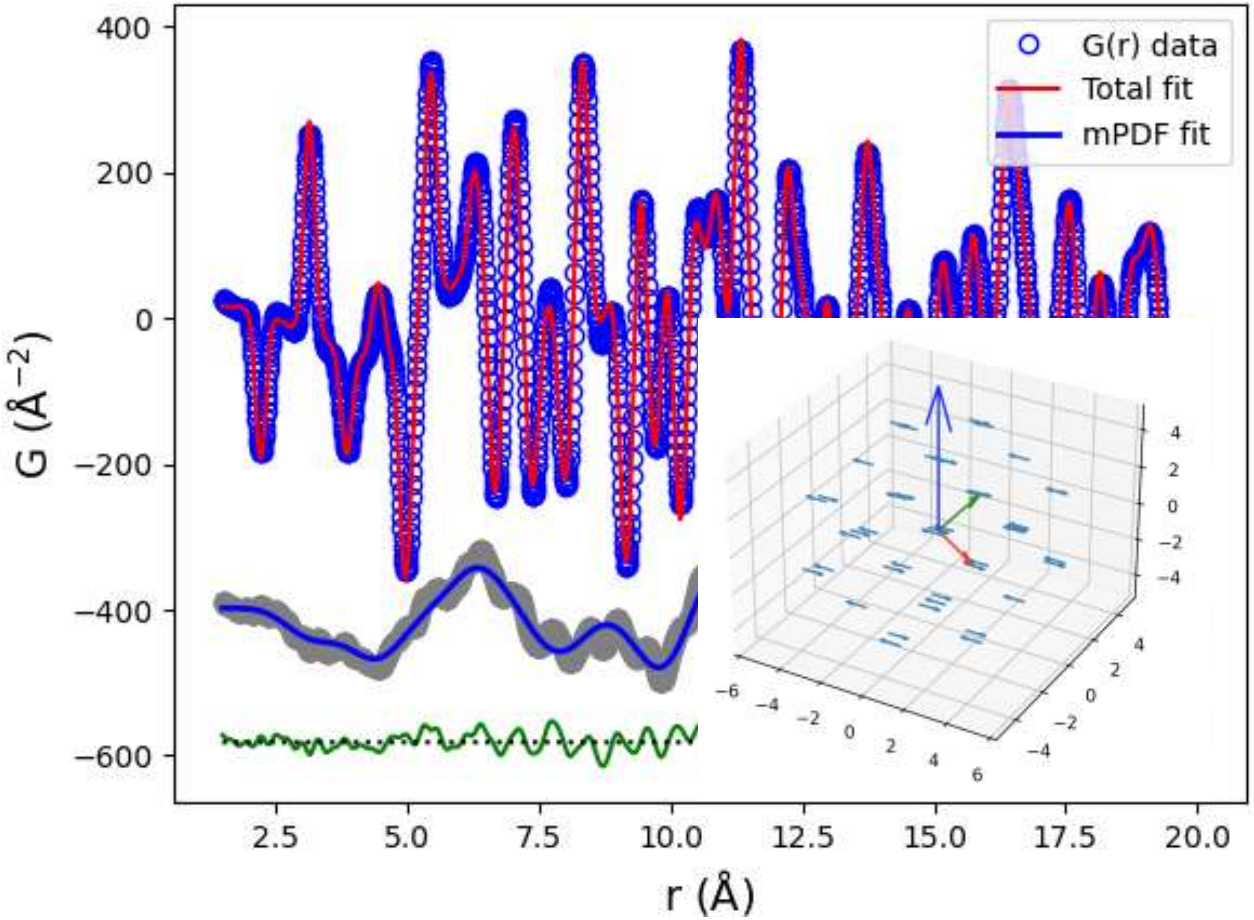

Toggle

R_w = 0.085

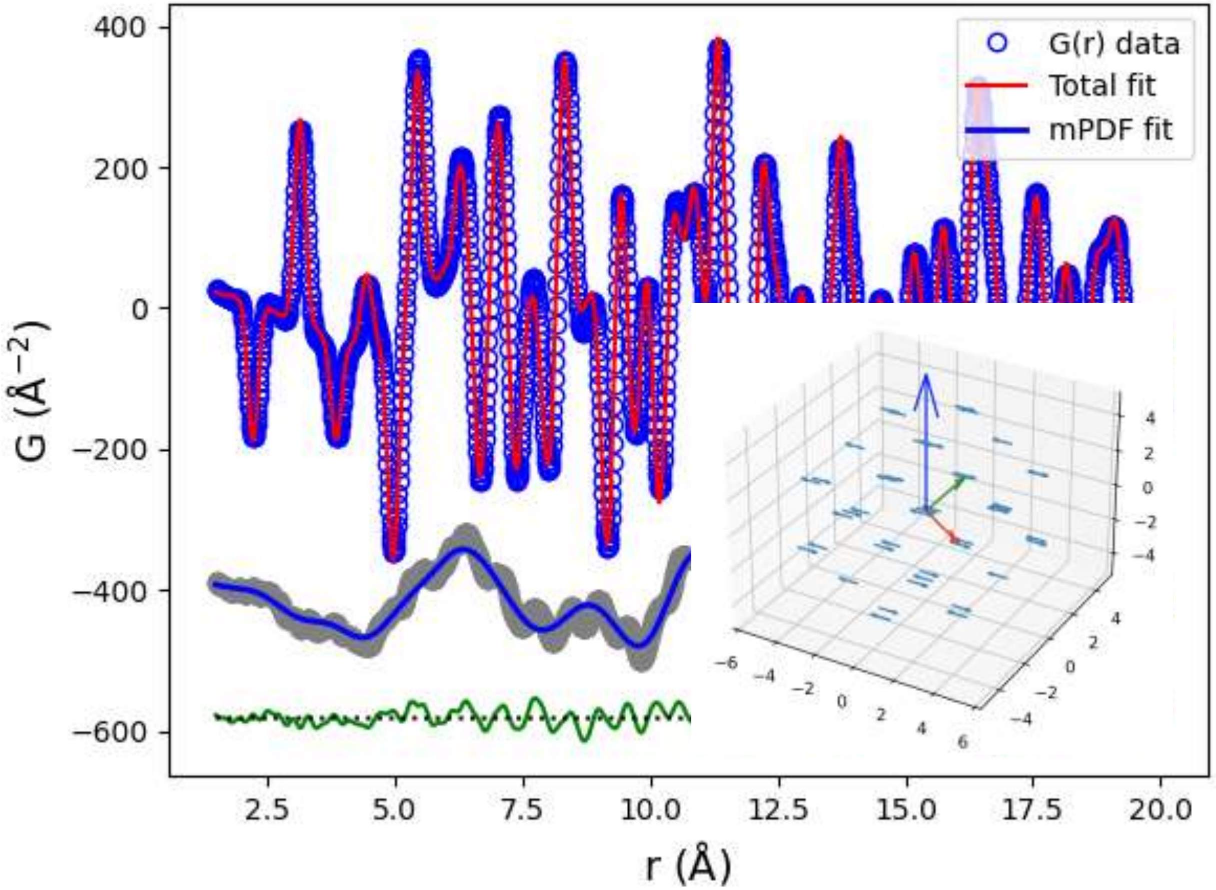

- **Co-refinement and toggle algorithms perform similarly well.**

Different Q_{max}

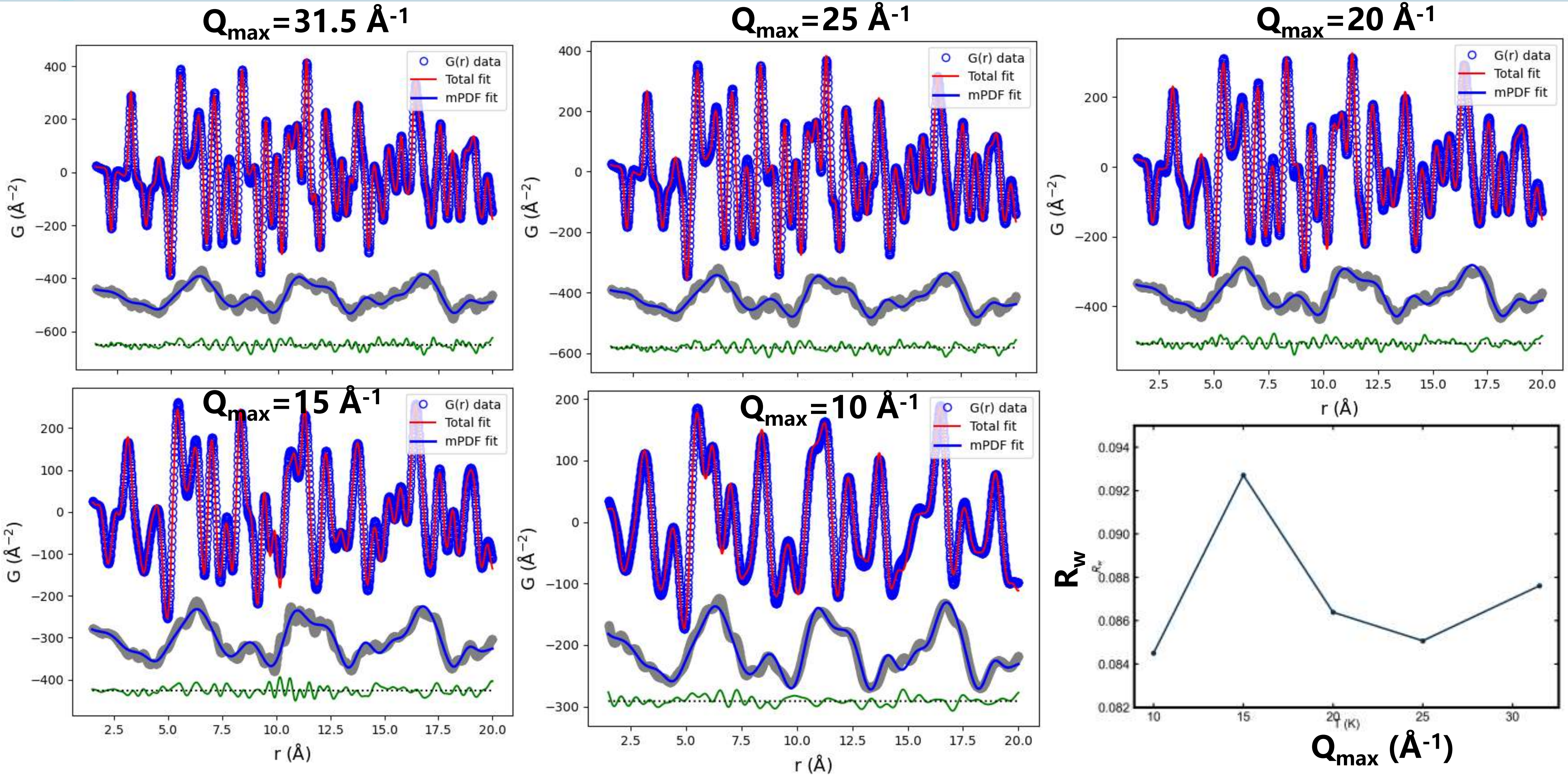

Lorch function

No lorch

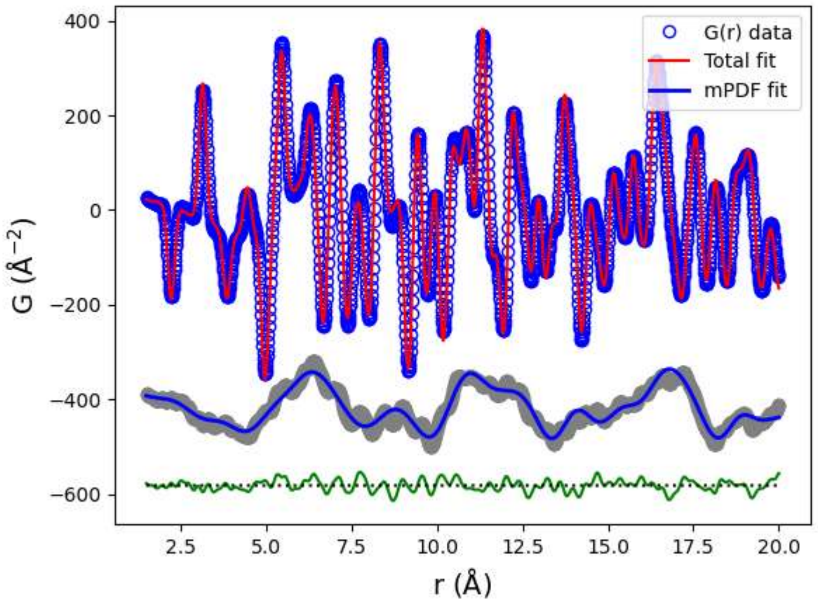

Q_{max} = 25 Å^{-1}
R_w= 0.100

Lorch

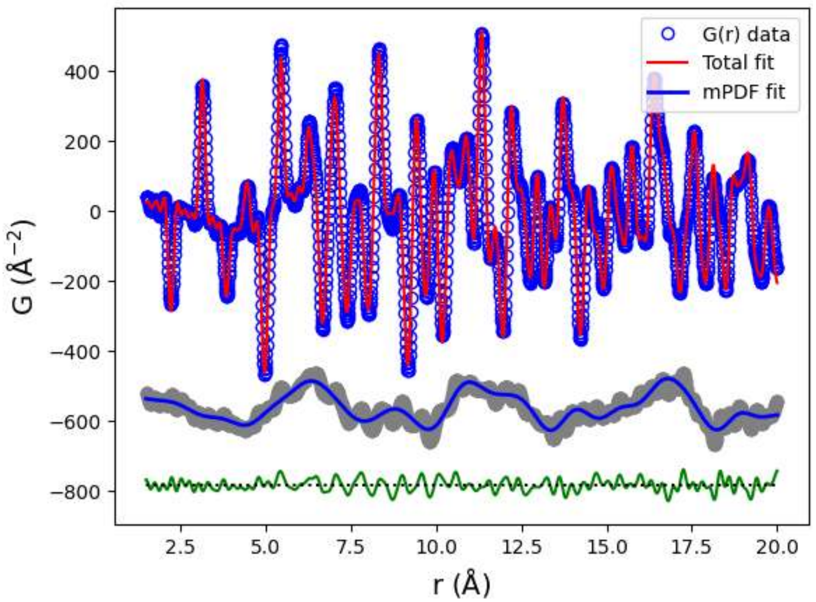

Q_{max} = 25 Å^{-1}
R_w= 0.085

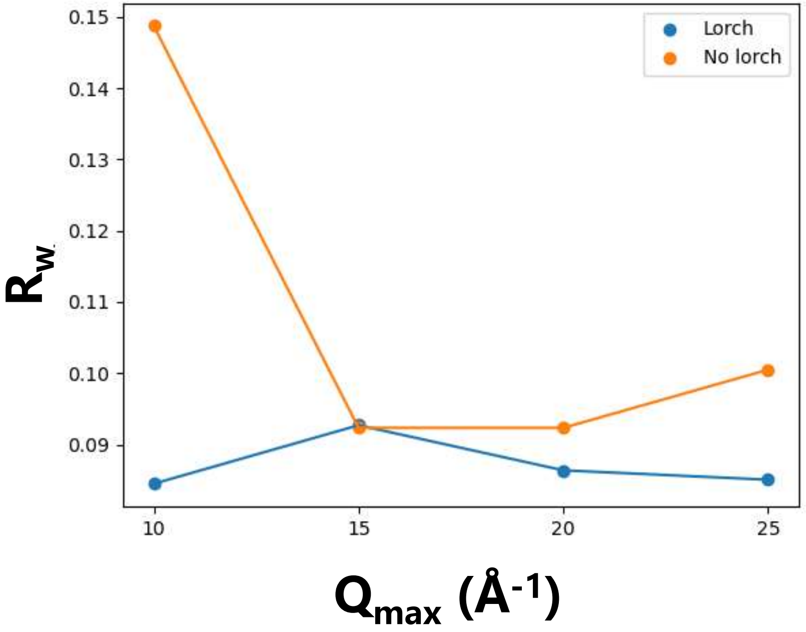

MnTe

- **Short-range antiferromagnetic correlations enhanced thermoelectric material.**

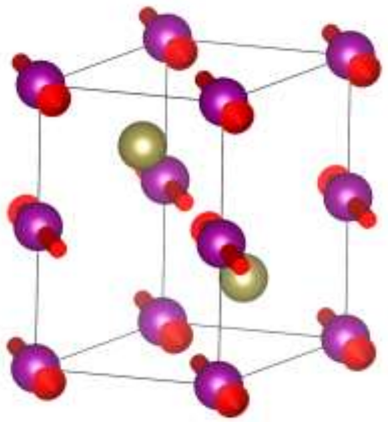

antiferromagnetic

Néel temperature 307 K

heating

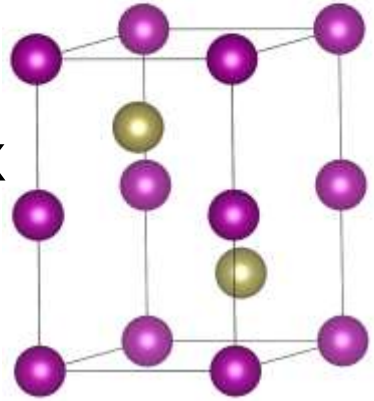

paramagnetic

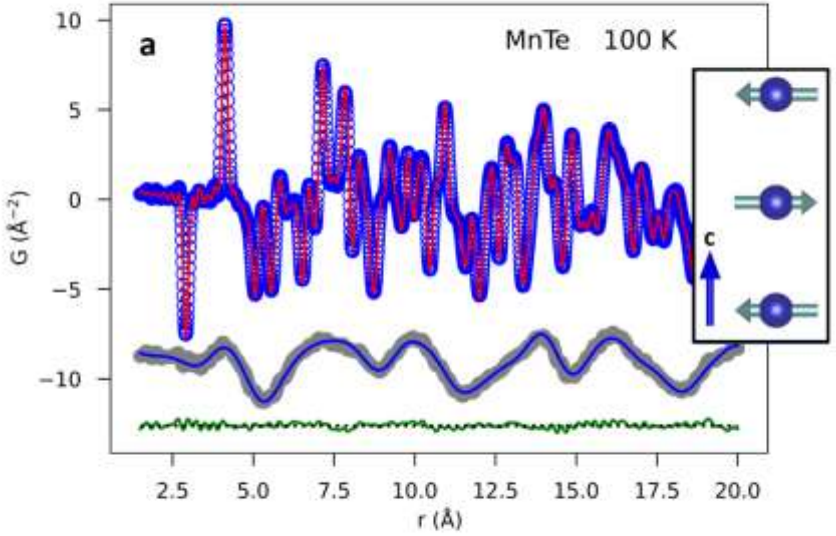

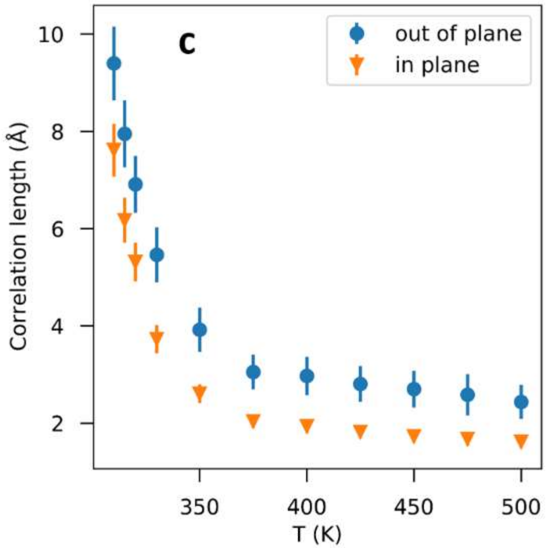

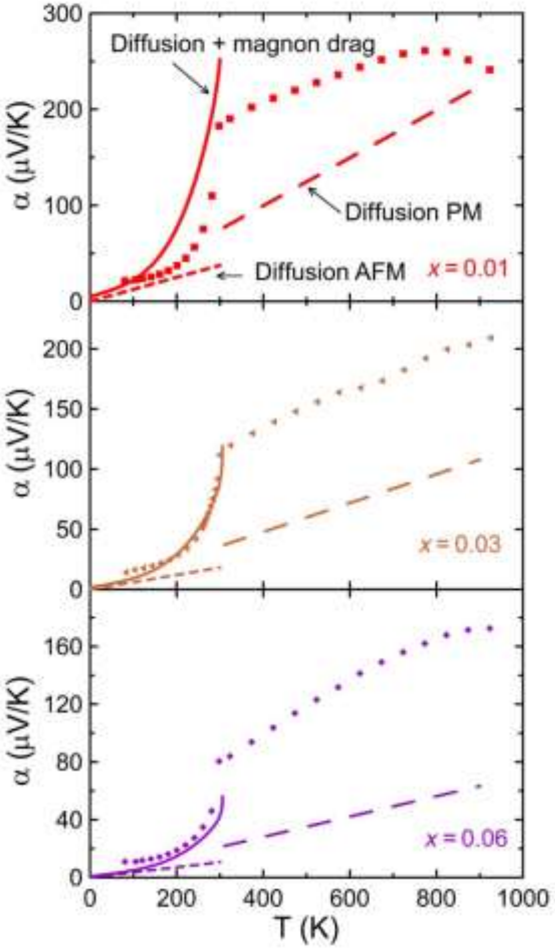

R. Baral, et al., *Matter*, 2022, 5, 6.
Y. Zheng, et al., *Sci. Adv.*, 2019, 5, 9.

Different exposure time

20 K

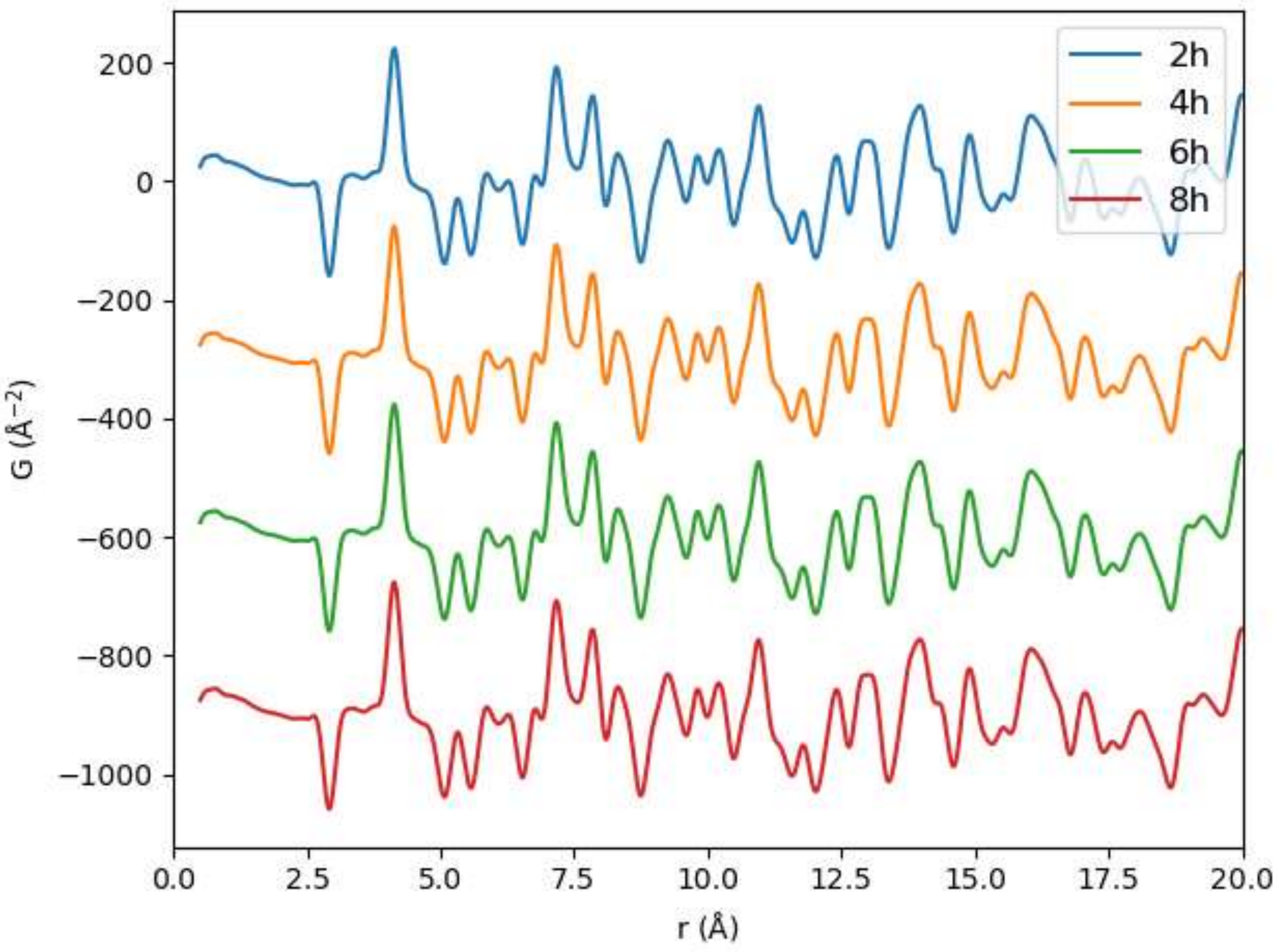

@MPI

MnTe - different exposure time

8h
R_w = 0.113

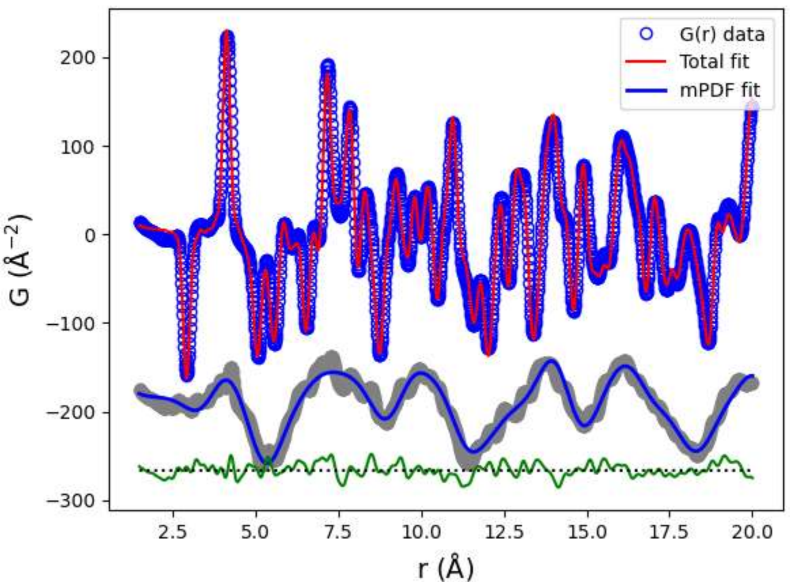

6h
R_w = 0.114

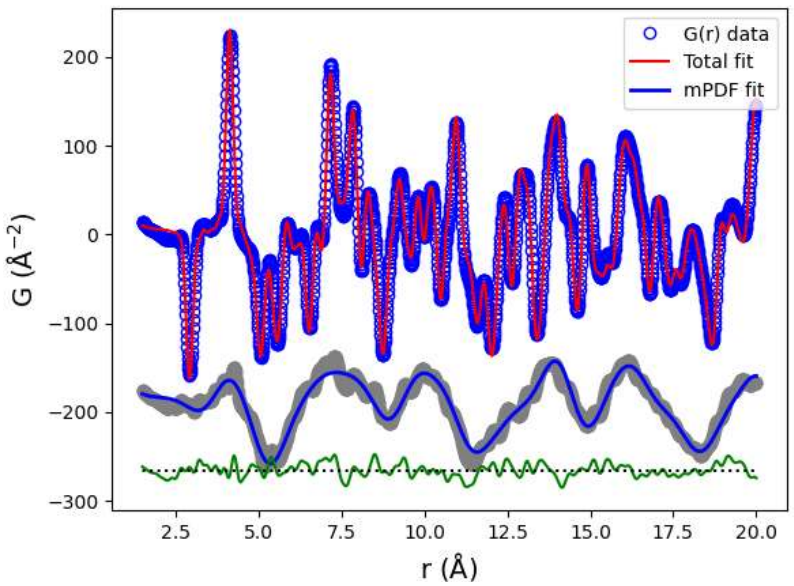

2h
R_w = 0.113

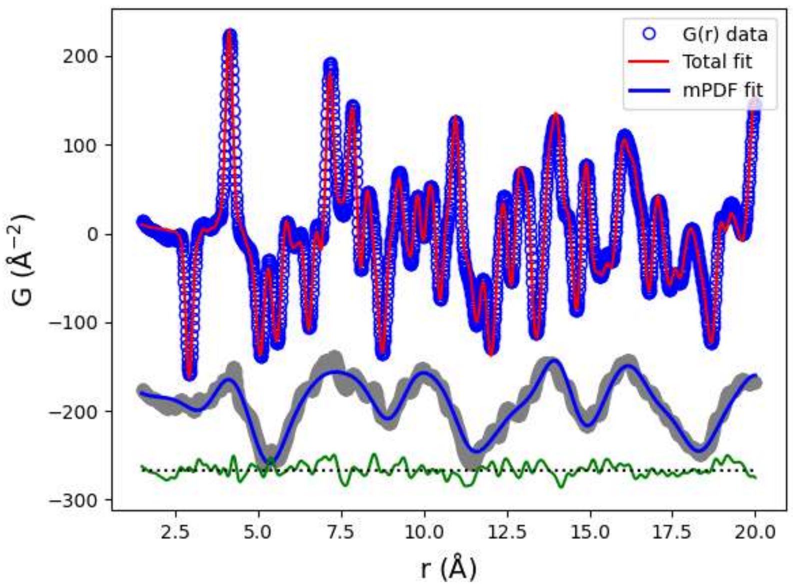

MnTe - different exposure time

20 K	8h	6h	2h
a (Å)	4.138	4.138	4.139
c (Å)	6.682	6.682	6.680
U_{Mn11} (Å^2)	0.0067	0.0068	0.0068
U_{Mn33} (Å^2)	0.0132	0.0132	0.0124
U_{O11} (Å^2)	0.0055	0.0055	0.0055
U_{O33} (Å^2)	0.0068	0.0067	0.0066
Corr. L (Å)	>1000	>1000	>1000
R_w	0.113	0.114	0.113

- **High-quality mPDF data can be collected in 2 hours at MPI.**

MnTe

Same exposure time

20K

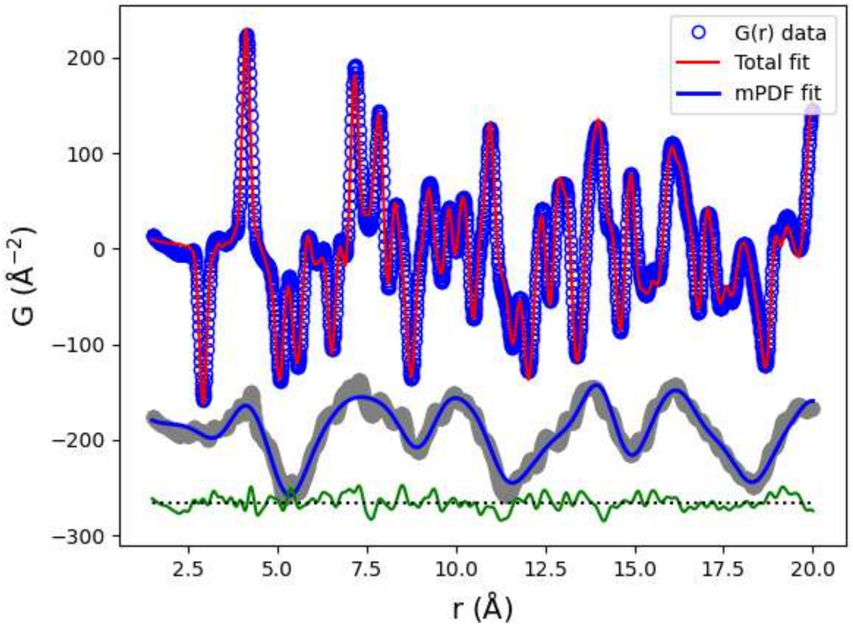

100K

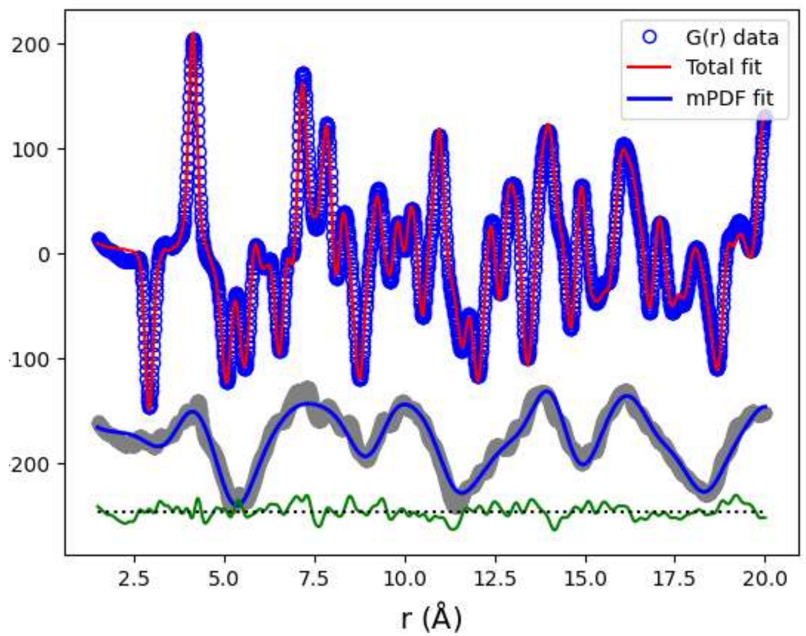

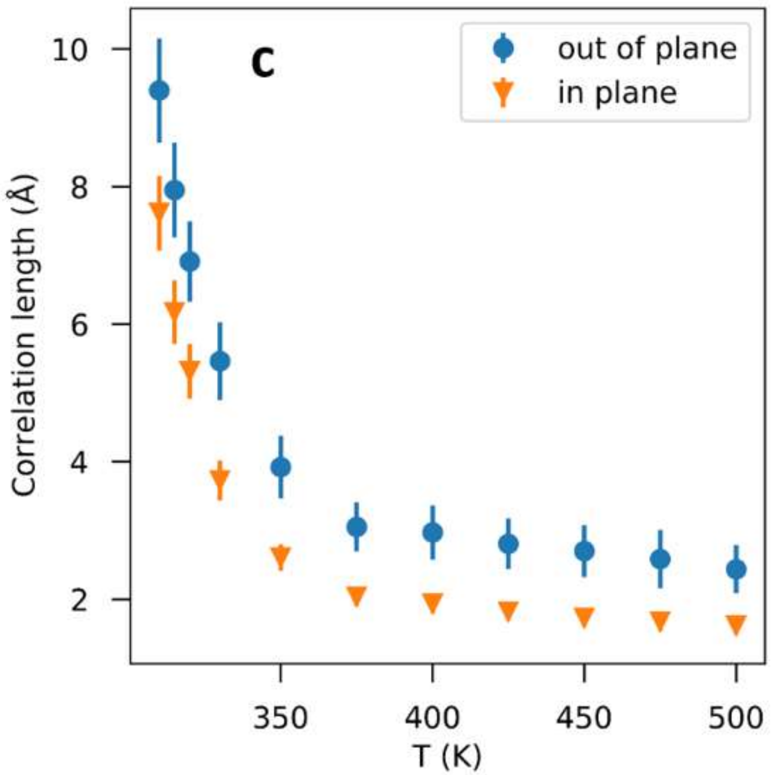

- **The short-range antiferromagnetic correlation persists above Néel temperature.**

DiffPy

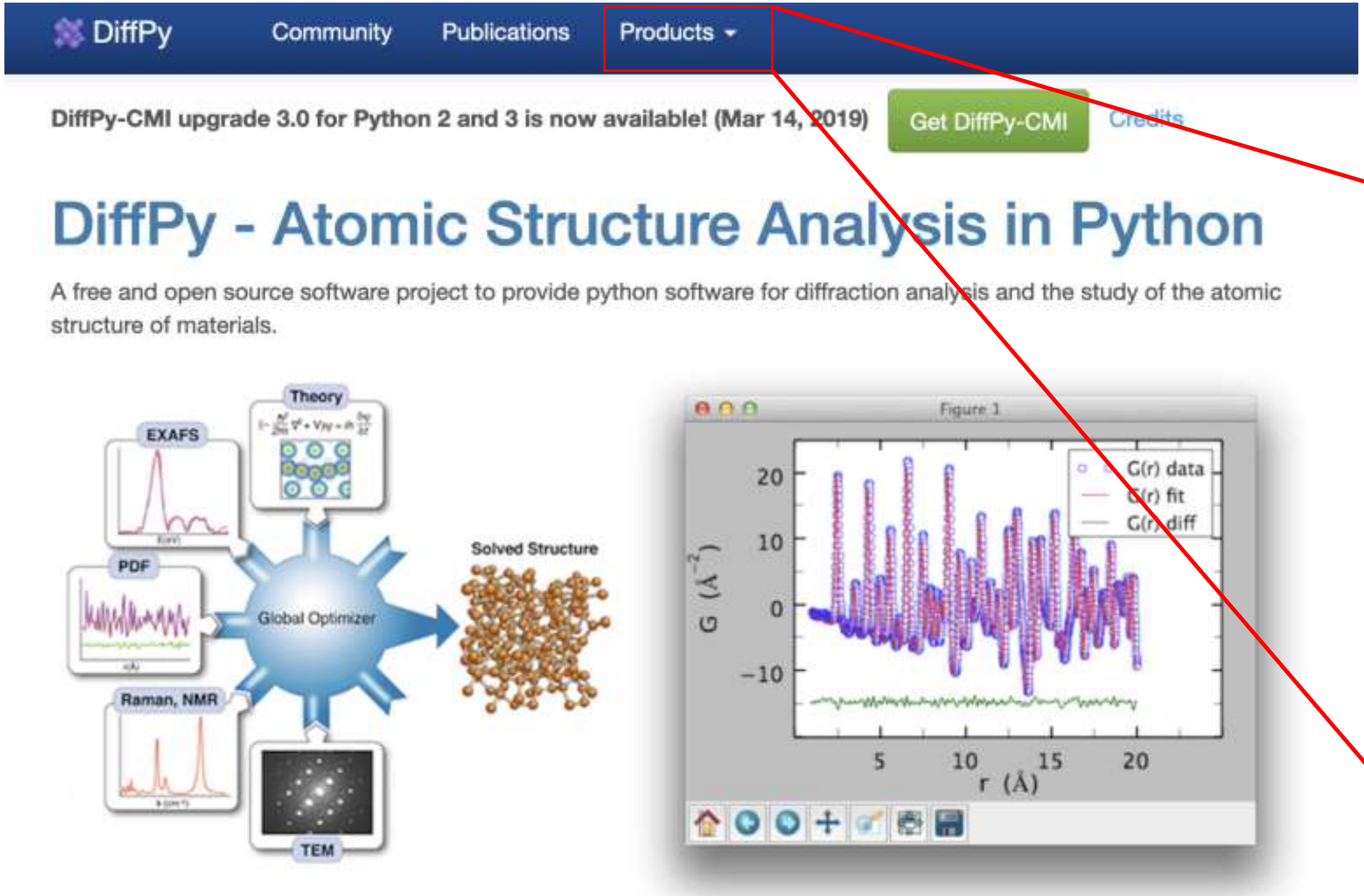

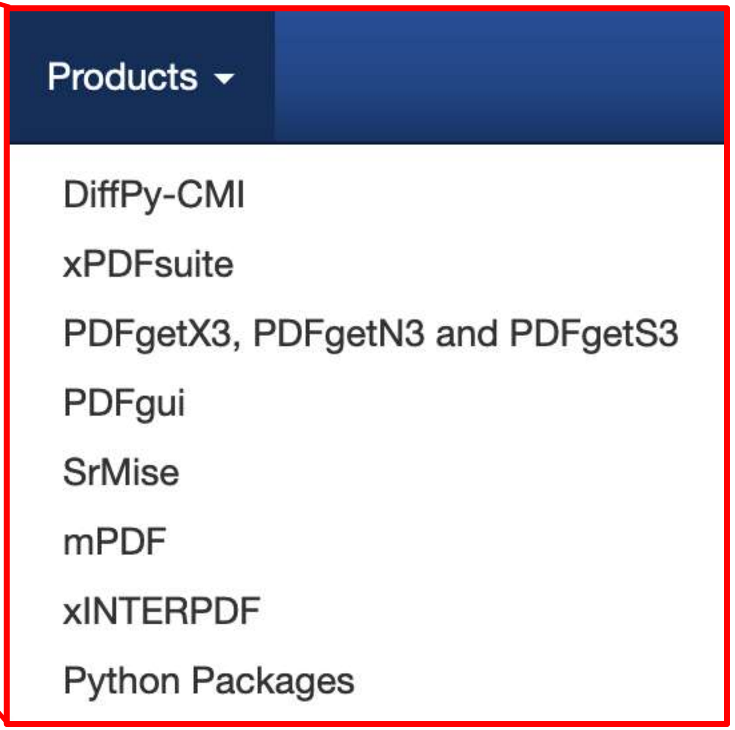

Release of PDFgui 2.0

https://diffpy.org

PDFgui 2.X

- **Support mPDF refinement**
- **UI visualize magnetic structure**

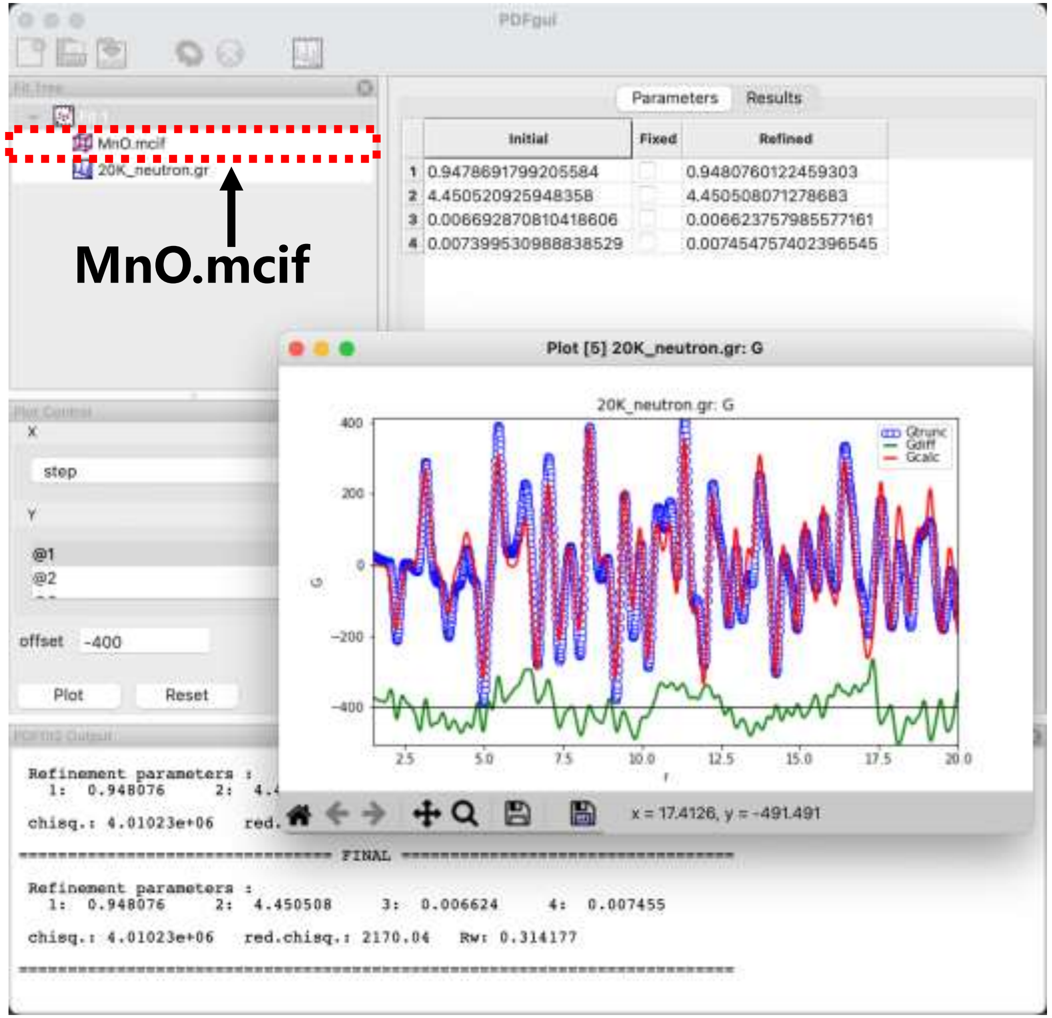

PDF in the Cloud

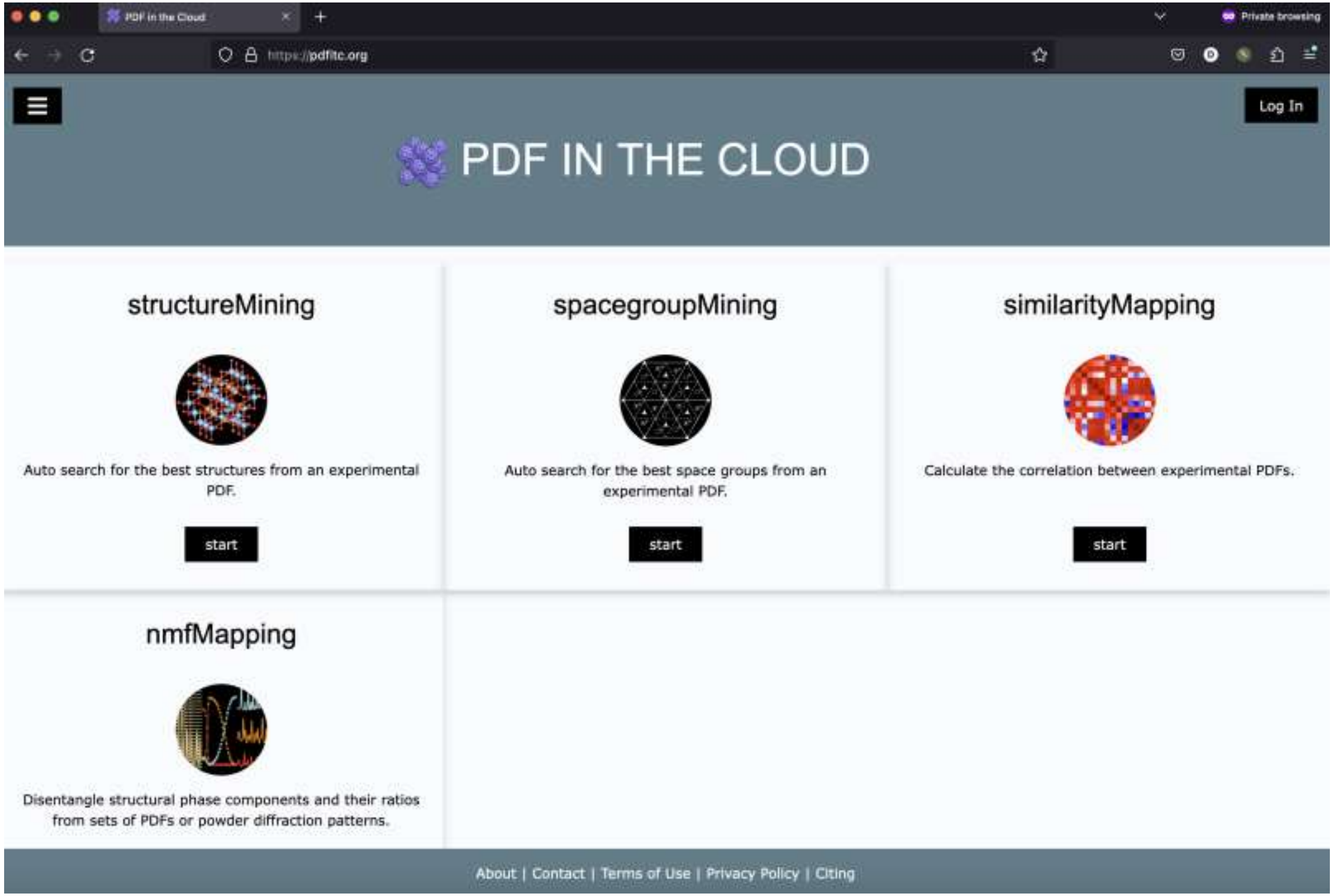

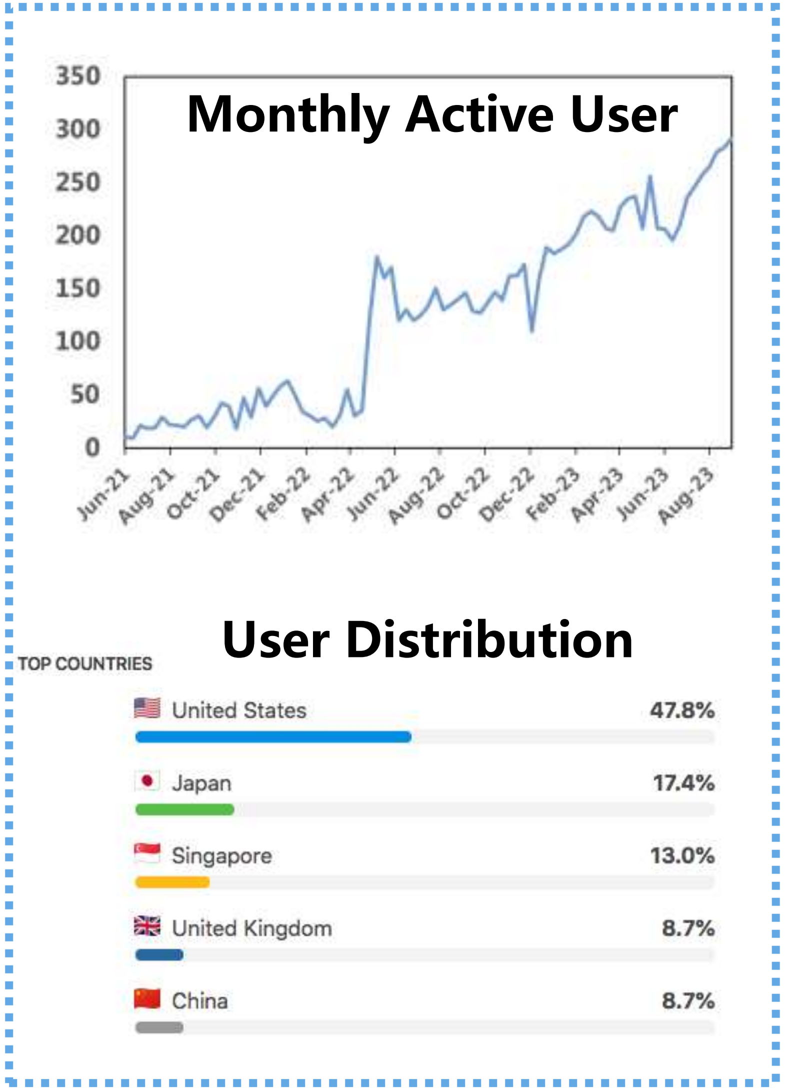

https://pdfitc.org

L. Yang, et al. Acta Crystallogr. A (2021)

Summary

- The MPI instrument is capable of collecting high quality mPDF data.
- The mPDF may serve as a promising method for exploring local magnetic correlations in complicated condensed matters.

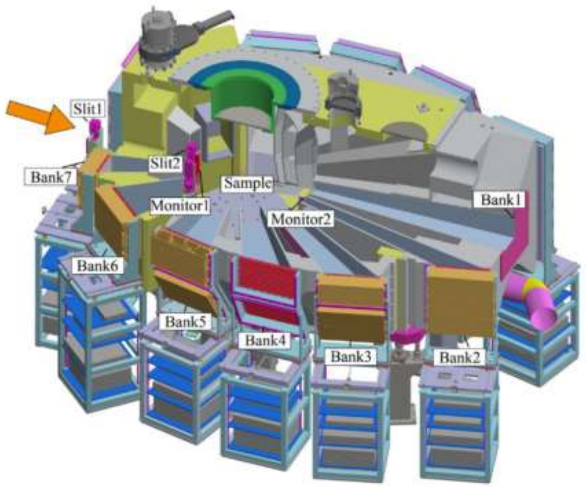

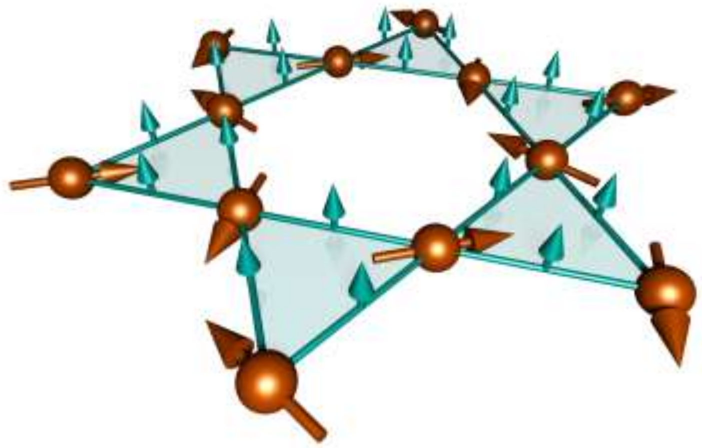

Thank you!

MnO

- **Early neutron diffraction studies showed that MnO has the cubic rock-salt structure (s.g.: Fm-3m) at high temperature, and rhombohedral phase (s.g.: R-3m) at low temperature. (Shull et al., 1951; Roth, 1958)**
- **The antiferromagnetic spin arrangement in MnO is compatible only with monoclinic or lower symmetry (Shaked et al., 1988), so the true structural symmetry must be lower than R-3m.**

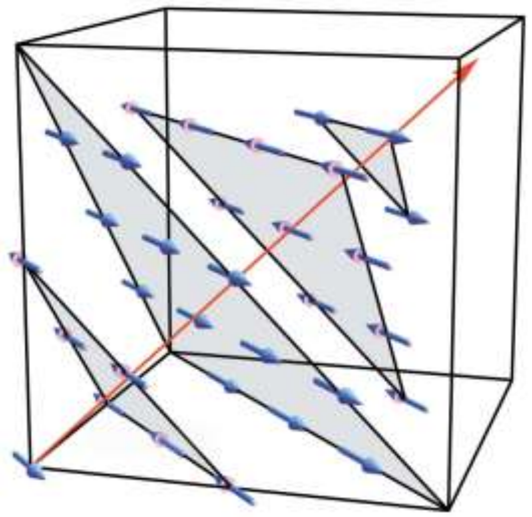

MnO

- In 1949 Clifford Shull and Ernest Wollan showed the magnetic structure of MnO, which leads to the discovery of antiferromagnetism.
- The spin alignment axis lies within the (111) plane, and the spin direction reverses between adjacent sheets along the [111] direction.
- Clifford Shull won the Nobel Prize in Physics in 1994.

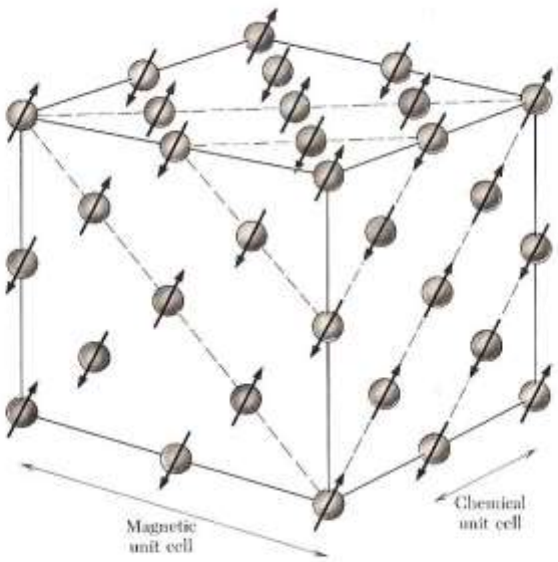

courtesy of ORNL

MnTe

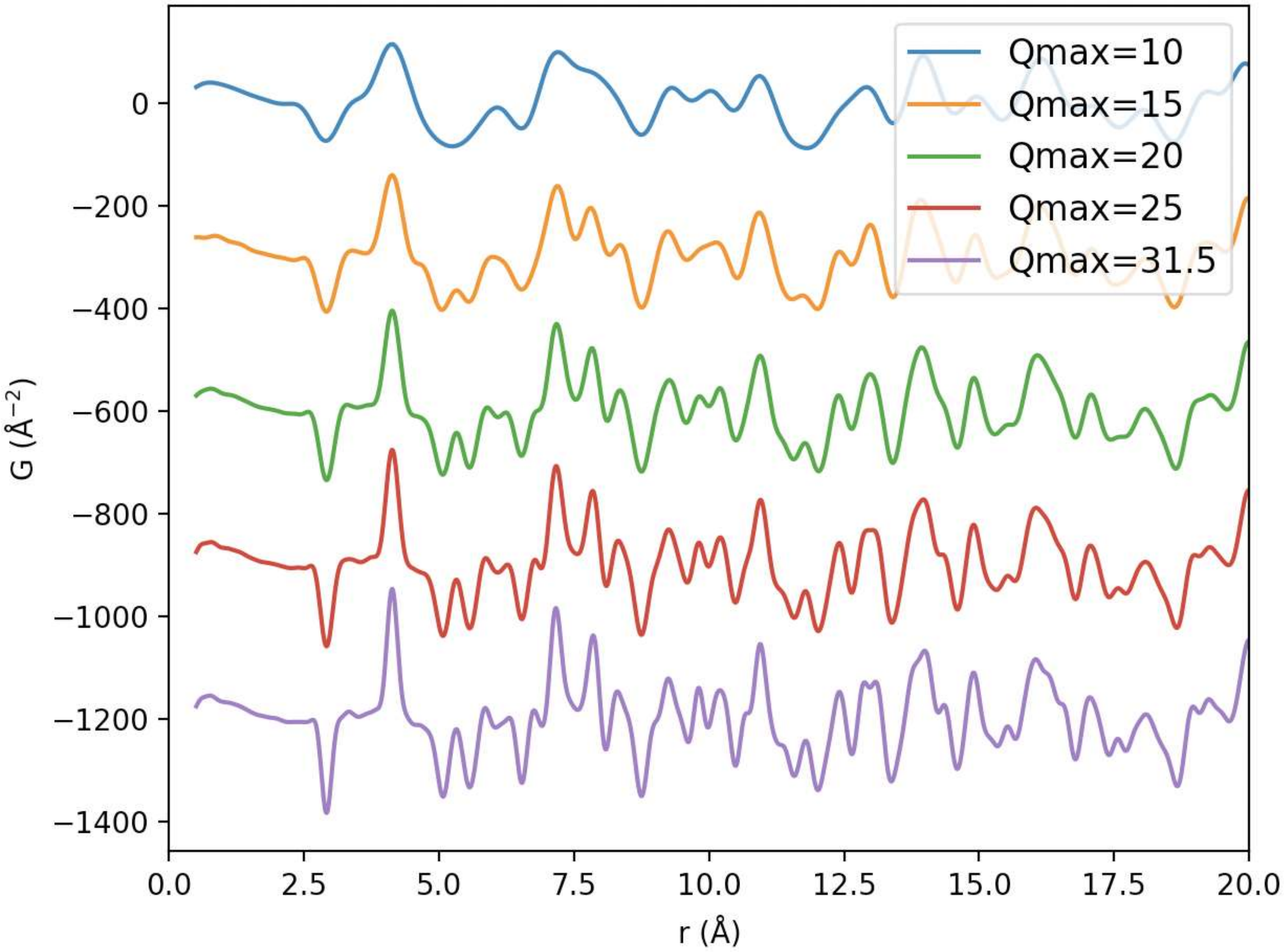

Qmax=10
Qmax=15
Qmax=20
Qmax=25
Qmax=31.5
0
−200
−400
−600
−800
−1000
−1200
−1400
G (Å⁻²)
0.0
2.5
5.0
7.5
10.0
12.5
15.0
17.5
20.0
r (Å)

Atomic v.s. magnetic PDF

- **mPDF is lower in frequency and characteristically broader than the atomic PDF due to the effects of the magnetic form factor.**
- **mPDF changes more dramatically with temperature.**

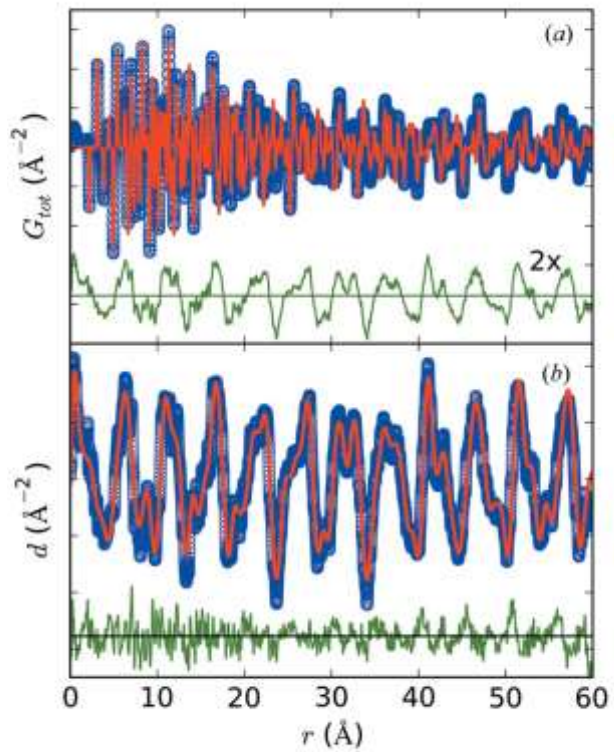

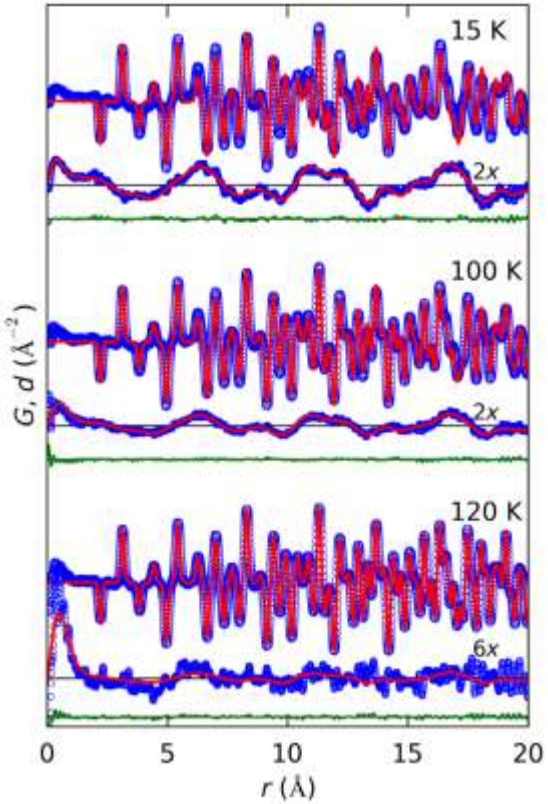

B. Frandsen, S. J.L. Billinge, *Acta Cryst. A*, 2015, 71, 3.
B. Frandsen, et al., *Phys. Rev. Lett.*, 2016, 116, 19.

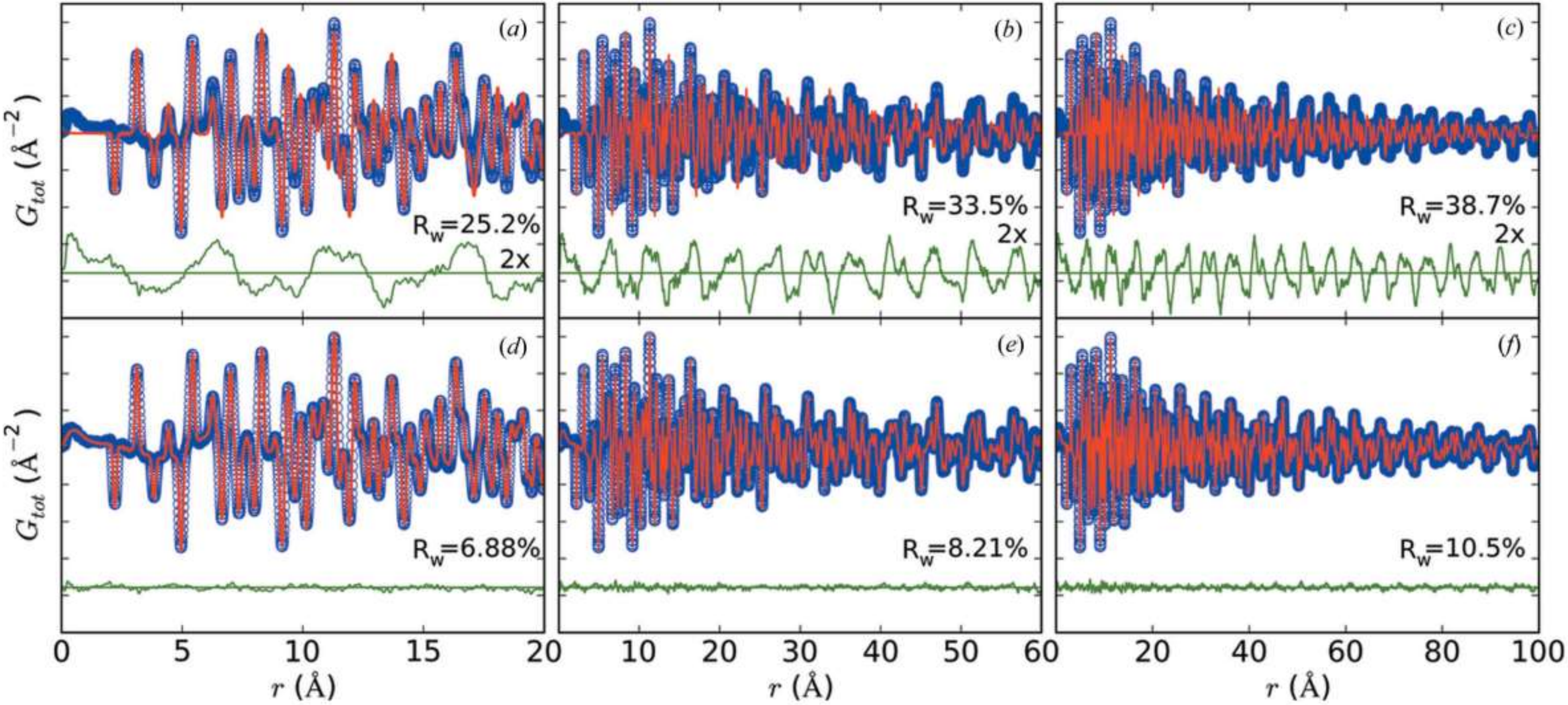

Figure 7

Save the figure

Atomic and magnetic PDF refinements of the monoclinic model for three fitting ranges. (*a*)–(*c*) Refinement results when only the atomic structure is included in the model. The mPDF $d(r)$ is seen in the difference curves, which are multiplied by two for clarity. (*d*)–(*f*) Results of co-refinements of the atomic and magnetic PDFs. In all panels, the blue curve is the experimental data, the red curve is the calculated pattern, and the offset green curve is the difference.

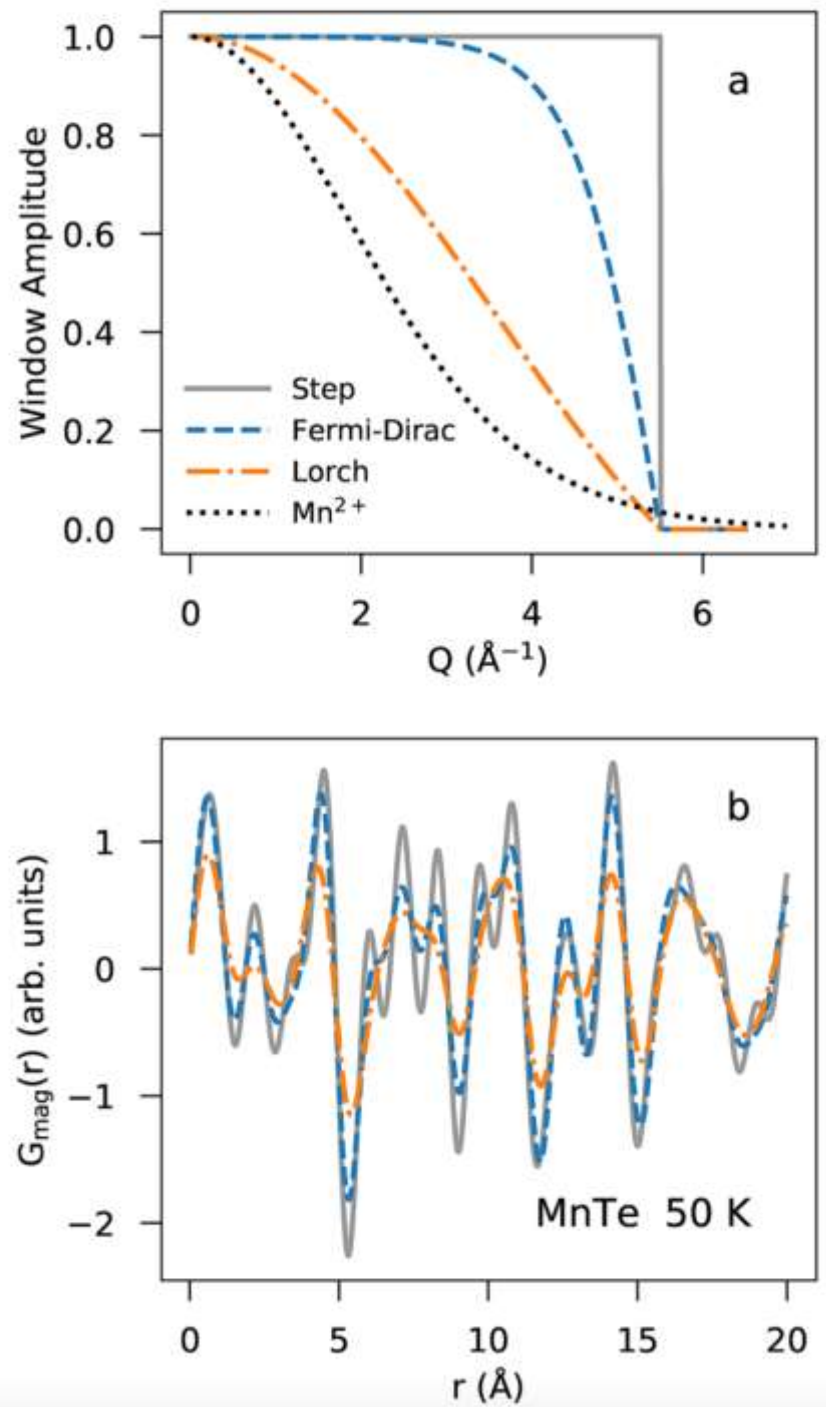

step function

$$w_s(Q) = \begin{cases} 1 & \text{if } Q \leq Q_{max}, \\ 0 & \text{if } Q > Q_{max}, \end{cases} \tag{6}$$

a modified Fermi–Dirac function

$$W_{FD}(Q) = \begin{cases} \frac{2}{e^{(Q-Q_{max})/\Delta}+1} - 1 & \text{if } Q \leq Q_{max}, \\ 0 & \text{if } Q > Q_{max}, \end{cases} \tag{7}$$

and the conventional Lorch function[33]

$$w_L(Q) = \begin{cases} \frac{Q_{max}}{\pi Q} \sin\left(\frac{\pi Q}{Q_{max}}\right) & \text{if } Q \leq Q_{max}, \\ 0 & \text{if } Q > Q_{max}. \end{cases} \tag{8}$$

B. Frandsen, et al., *J Appl. Phys.*, 2022, 132, 22.

Co-refinement v.s. Toggle

20 K	no mPDF fit	Co-refine mPDF fit	Toggle mPDF fit
a (Å)	3.161	3.161	3.161
c (Å)	7.628	7.619	7.618
U_{Mn11} (Å^2)	0.0050	0.0056	0.0056
U_{Mn33} (Å^2)	0.0044	0.0066	0.0064
U_{O11} (Å^2)	0.0061	0.0060	0.0051
U_{O33} (Å^2)	0.0057	0.0063	0.0066
R_w	0.30	0.086	0.085

- **Co-refinement and toggle algorithms perform similarly well.**

MnO 20K-300K

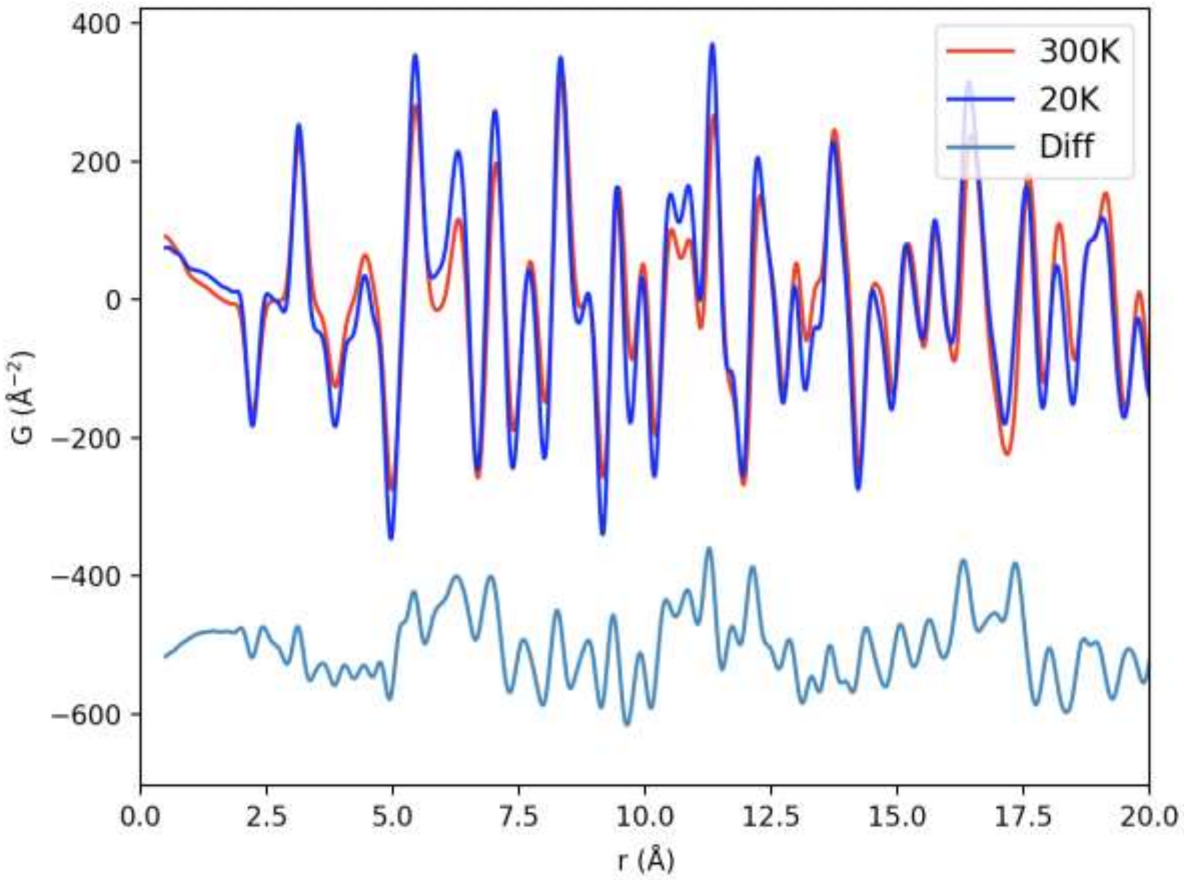

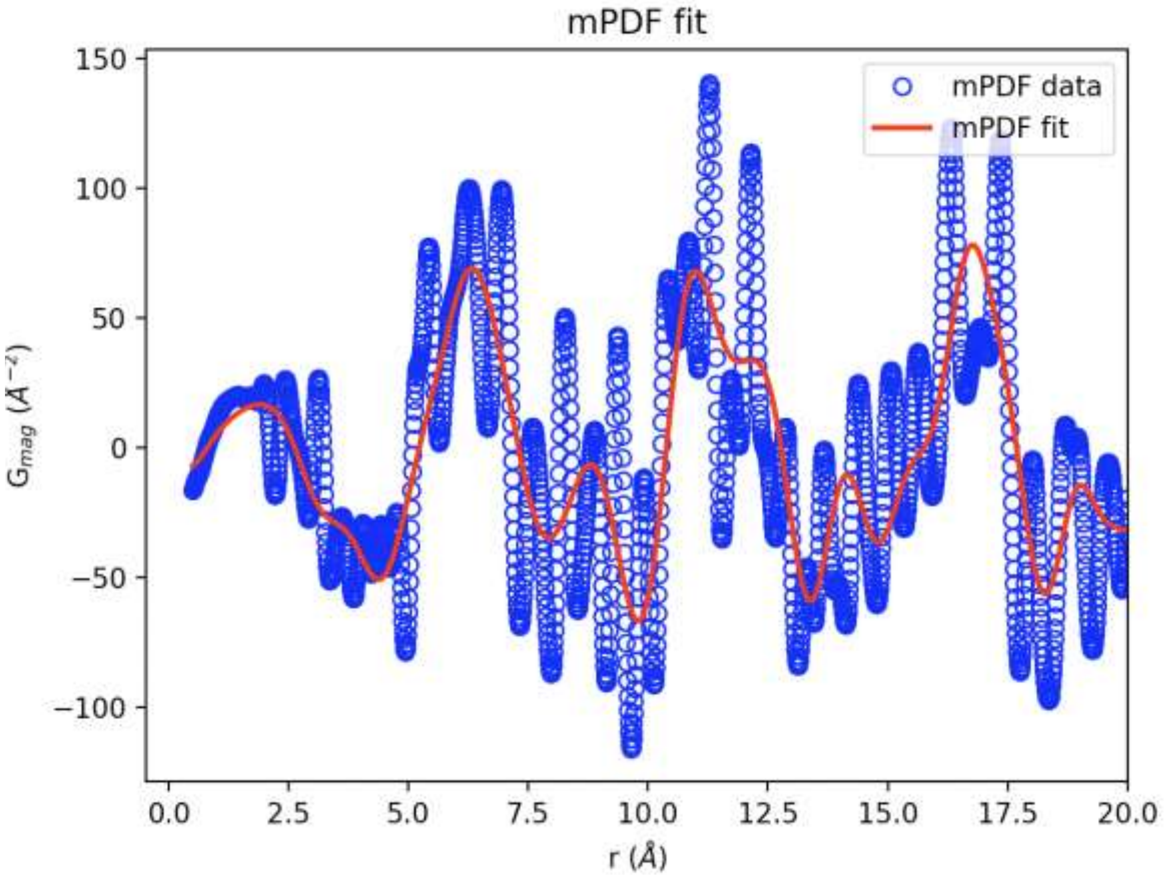

Q_{max}=25 $Å^{-1}$, Use Lorch

mPDF

$$G_{\text{tot}}(r) = \mathcal{F}\left\{Q\left(\frac{I_{\text{n}}}{N_{\text{a}}\langle b\rangle^2} - \frac{\langle b^2\rangle}{\langle b\rangle^2}\right)\right\} + \mathcal{F}\left\{Q\frac{I_{\text{m}}}{N_{\text{a}}\langle b\rangle^2}\right\}$$
$$= G_{\text{n}}(r) + d(r)/N_{\text{a}}\langle b\rangle^2,$$

where $G_{\text{n}}(r)$ is the atomic (nuclear) PDF and $d(r) = \mathcal{F}\{QI_{\text{m}}(Q)\}$ is a quantity that we will call the 'unnormalized mPDF', since it does not involve division by the magnetic form factor $f_{\text{m}}(Q)$. A straightforward application of the convolution theorem reveals that

$$d(r) = C_1 \times f(r) * S(r) + C_2 \times \frac{\mathrm{d}S}{\mathrm{d}r},$$

where C_1 and C_2 are constants related by $C_1/C_2 = -1/(2\pi)^{1/2}$ in the fully ordered state, $*$ represents the convolution operation, and $S(r) = \mathcal{F}\{f_{\text{m}}(Q)\} * \mathcal{F}\{f_{\text{m}}(Q)\}$. The quantity $\mathcal{F}\{f_{\text{m}}(Q)\}$ is closely related to the real-space spin density. Roughly speaking, $d(r)$ is equivalent to the proper mPDF $f(r)$ twice broadened by the spin density with an additional peak at low r produced by the derivative term in equation (6). The two